Investigating Late Amazonian Volcanotectonic Activity on Olympus Mons, Mars Using Flank Vents and Arcuate Graben

by

Sean I. Peters

A Thesis Presented in Partial Fulfillment
of Requirements for the Degree
Master of Science

Approved May 2015 by the
Graduate Supervisory Committee:

Philip Christensen, Chair
Amanda Clarke
Kelin Whipple

ARIZONA STATE UNIVERSITY

August 2015

ABSTRACT

Olympus Mons is the largest volcano on Mars. Previous studies have focused on large scale features on Olympus Mons, such as the basal escarpment, summit caldera complex and aureole deposits. My objective was to identify and characterize previously unrecognized and unmapped small scale features to understand the volcanotectonic evolution of this enormous volcano. For this study I investigated flank vents and arcuate graben. Flank vents are a common feature on composite volcanoes on Earth. They provide information on the volatile content of magmas, the propagation of magma in the subsurface and the tectonic stresses acting on the volcano. Graben are found at a variety of scales in close proximity to Martian volcanoes. They can indicate flexure of the lithosphere in response to the load of the volcano or gravitation spreading of the edifice. Using Context Camera (CTX), High Resolution Imaging Science Experiment (HiRISE), Thermal Emission Imaging System (THEMIS), High Resolution Stereo Camera Digital Terrain Model (HRSC DTM) and Mars Orbiter Laser Altimeter (MOLA) data, I have identified and characterized the morphology and distribution of 60 flank vents and 84 arcuate graben on Olympus Mons. Based on the observed vent morphologies, I conclude that effusive eruptions have dominated on Olympus Mons in the Late Amazonian, with flank vents playing a limited role. The spatial distribution of flank vents suggests shallow source depths and radial dike propagation. Arcuate graben, not previously observed in lower resolution datasets, occur on the lower flanks of Olympus Mons and indicate a recent extensional state of stress. Based on spatial and superposition relationships, I have constructed a developmental sequence for the construction of Olympus Mons: 1) Construction of the shield via effusive lava flows.; 2) Formation of

the near summit thrust faults (flank terraces); 3) Flank failure leading to scarp formation and aureole deposition; 4) Late Amazonian effusive resurfacing and formation of flank vents; 5) Subsidence of the caldera, waning volcanism and graben formation. This volcanotectonic evolution closely resembles that proposed on Ascraeus Mons. Extensional tectonism may continue to affect the lower flanks of Olympus Mons today.

ACKNOWLEDGEMENTS

I would like to thank Phil Christensen, Amanda Clarke, Kelin Whipple and Paul Byrne for helpful discussions and constructive feedback. I would also like to thank Jacob Bleacher and Jacob Richardson for introducing me to the Catalogue of Tharsis Small Volcanic Vents dataset and providing helpful discussion.

TABLE OF CONTENTS

Page

Page

LIST OF TABLES

Table Page

LIST OF FIGURES

Figures Page

1.Introduction

Volcanism has played a fundamental role in creating and shaping the Martian crust [Carr, 1973; Carr et al., 1977; Greeley and Spudis, 1981; Wilson and Head, 1994; Wilson and Head, 2002; Werner, 2009]. Approximately 60% of the planet has been resurfaced by volcanism [Greeley and Spudis, 1981]. A variety of volcanic landforms are observed on the Martian surface, including the massive shields of the Tharsis volcanic province, the highland patera, and the young flows of Cerberus Fossae [Carr, 1973; Carr et al., 1977; Greeley and Spudis, 1981; Plescia, 2004; Werner, 2009]. The trend in volcanism in Martian history has been one of decreasing spatial and temporal activity [Greeley and Spudis, 1981; Werner, 2009]. Additionally, there is a complex interplay between volcanism and tectonism on Mars. In many locations on Mars, linear graben observed cutting the landscape are interpreted as the surface expression of dikes [Carr, 1974; Head and Wilson, 2002]. On the other hand, arcuate, or concentric, graben observed on the flanks of Ascraeus Mons (one of the Tharsis Montes) might indicate gravitational spreading or flexure of the edifice [Byrne et al., 2012, Pozzobon et al., 2015]. By studying flank vents and arcuate graben on Olympus Mons, I have characterized Late Amazonian volcanic activity, recent deformation on the shield, and constructed a relative geologic history of Olympus Mons. These data place constraints on the state of stress and the magma plumbing system.

2.Olympus Mons

Olympus Mons, an enormous shield volcano, stands approximately 22 km high and has basal dimensions of approximately 800 x 600 km [Carr, 1973; Blasius and Cutts,

1981; Greeley and Spudis, 1981; Plescia 2004; Werner, 2009]. Olympus Mons is situated in the Tharsis province just off the Tharsis Bulge, northwest of the Tharsis Montes and southwest of Alba Mons (Fig. 1). The shield host a variety of perplexing and enormous geologic features (Fig. 2). At the summit, a nested caldera complex approximately 90 x 60 km [Carr, 1973; Wood, 1984; Mouginis-Mark and Rowland, 2001; Plescia, 2004]. A basal escarpment ranging in height from 3 – 8 km wraps around the entire shield [Carr, 1973; King and Riehle, 1974; Carr et al., 1977; Tanaka, 1985; Thomas et al., 1990; Milkovich et al., 2006]. To the northeast and southwest, lava flows have draped over the escarpment and obscured its topographic expression [Carr et al., 1977; Greeley and Spurdis, 1981]. These lava flows have created two distinct aprons that increased the apparent size of the shield post-escarpment formation. To a lesser extent lava has flowed off the escarpment to the south. Most of the flows off the shield are embayed by flows from Tharsis. Aureole deposits, interpreted as massive landslides derived from the volcano via flank failure, extend up to 800 km away from Olympus Mons [Carr, 1973; King and Riehle, 1974; Carr et al., 1977; Tanaka, 1985; Thomas et al., 1990; McGovern et al., 2004; Mouginis-Mark and Christensen, 2005]. Convex-up, fish-scale topography, known as flank terraces, observed on the upper flanks of the shield are thought to represent thrust faulting due to flexure of the edifice [Carr et al., 1977; Thomas et al., 1990; McGovern and Solomon, 1993; Byrne et al., 2009; Byrne et al., 2012]. Despite its size and scale, Olympus Mons displays gentle slopes of ~3 – 5 degrees over much of its flanks, with steeper slopes (~25 – 35 degrees) restricted to the basal escarpment [King and Riehle, 1974; Blasius and Cutts, 1981; Plescia, 2004]. The morphology of Olympus Mons and its resemblance to the Hawaiian shields has been used

to infer a basaltic composition for its erupted lavas [Carr, 1973; Wood, 1984; Hulme, 1976; Zuber and Mouginis-Mark, 1992; Bleacher et al., 2007]. Although Olympus Mons probably started its construction during the Early Hesperian (~3.8 Ga), the flanks of the volcano have been dated to the Late Amazonian (~150 – 700 Ma) [Neukum et al., 2004; Werner, 2009; Tanaka et al., 2014]. Effusive activity has dominated in the Late Amazonian as evidenced by abundant lava tubes and channels [Carr, 1973; Carr et al., 1977; Neukum et al., 2004; Bleacher et al., 2007; Werner, 2009]. Some of the youngest features on Olympus Mons are the nested calderas (~100 – 200 Ma) and flows on the southwestern flanks (≤ 50 Ma) [Neukum et al., 2004; Werner, 2009; Tanaka et al., 2014]. A few locations on the shield are significantly older (~3.8 Ga) and may represent an ancient proto-Olympus Mons [Werner, 2009]. The shield is blanketed in 0.5 – 2 m of dust that prevents spectral analysis and obscures finer details of the topography [Christensen, 1986].

2.1 Flank Vents

Flank, or satellite, vents are a common feature on terrestrial composite volcanoes of various compositions [Nakamura, 1977; Wood, 1980; Davidson and DeSilva, 2000; Corrazato and Tibaldi, 2006]. Examples include Cerro Azul (Galapagos Islands), Mount Etna and Santa Clara (Pinacates Volcanic Field, Mexico) [Nakamura, 1977; Rowland, 1996; Davidson and DeSilva, 2000; Corrazato and Tibaldi, 2006]. Vents can manifest as fissures, scoria cones, lava lakes and low shields [Greeley, 1977; Wood, 1980; Greeley, 1982; Rowland, 1996; Davidson and DeSilva, 2000; Corrazato and Tibaldi, 2006; Hauber et al., 2009; Brož and Hauber, 2012]. Flank vents provide crucial information about the evolution of a volcano. The type of vent provides information on the magma volatile

content, effusion rates and eruption style [Wood, 1980; Rowland, 1996; Davidson and DeSilva, 2000; Corrazato and Tibaldi, 2006]. The spatial distribution of flank vents provides information on the stress field acting on the volcano at the time of formation and the geometry of a volcano's plumbing system, specifically the direction and orientation of magma propagation and magma source depths [Nakamura, 1977; Bleacher et al., 2009; Hauber et al., 2009]. The relationship of flank vents to other prominent features can also help reconstruct the evolutionary sequence of the volcano [Byrne et al., 2012]. In the absence of geophysical, geothermal and spectral data for Olympus Mons, flank vents offer a powerful tool to understand its volcanic evolution.

2.2 Arcuate Graben

Graben are a common feature across the Tharsis volcanic province [Carr, 1974; Wilson and Head, 2002]. They are observed cutting across volcanic plains and even the Tharsis Montes [Carr, 1974; Wilson and Head, 2002; Byrne et al., 2012; Pozzobon et al., 2015]. Many are hypothesized to represent the surface expression of dike propagation [Wilson and Head, 2002]. Others, such as those observed on the Tharsis Montes, may reflect either gravitational spreading of the edifice or flexure of the edifice due to adjustment of the lithosphere to the load [McGovern and Solomon, 1993; Byrne et al., 2009; Byrne et al., 2012]. Smaller arcuate graben observed around the margin of volcanic edifices likely do not represent dike propagation [Byrne et al., 2012]. None of the arcuate graben display any evidence of a volcanic origin, such as emanating flows. These structures are more consistent with proposed flexure of the lithosphere due to the loading of the volcanic edifice or gravitational spreading of the edifice driven by self-loading [Byrne et al., 2009; Byrne et al., 2012; Pozzobon et al., 2015]. Superposition

relationships of graben and other features can provide a relative sequence of geologic events.

3.Methodology

I used image data from the Context Camera [CTX (~5 m/pixel), Malin et al., 2007], the Thermal Emission Imaging System [THEMIS (100 m/pixel), Christensen et al., 2004] and the High Resolution Imaging Science Experiment [HiRISE (0.25 – 0.32 m/pixel), McEwan et al., 2007]. For topographic and morphometric investigations, I utilized the Mars Orbital Laster Altimeter [MOLA, Zuber et al., 1992] and the High Resolution Stereo Camera Digital Terrain Models [HRSC DTM (cell size: ~50 m), Jaumann et al., 2007]. I mosaicked 159 Context Camera (CTX) images, with similar emission angles (~0-20 degrees) although higher emission angles were chosen in order to fill gaps in coverage. This high resolution dataset allowed for the identification and characterization of small morphologic features. After an initial survey to identify and locate flank vents, I utilized the Catalogue of Tharsis Small Volcanic Vents [Bleacher et al., 2010] to identify additional possible vents. I utilized HRSC DTMs, which provided partial coverage of Olympus Mons, to determine the heights of 22 vents and volume estimates for 18 others. The volumes were calculated by assuming a conical shape for cones and shields [Davidson and DeSilva, 2000; Hauber et al., 2009]. Although the vents occur on a sloped surface (~3 – 5 degrees) which will cause preferential flow downhill, I assumed negligible error due to this effect. Regional slopes on the edifice may result in lower edifice heights than those expected on a flat surface, since some volume erupted that would have contributed to its height instead contributes to its width. The formation

of cinder cones specifically is not affected by slopes less than 9 degrees [Broz and Hauber, 2012] although greater slopes are present on the escarpment. Graben were primarily visible in CTX and measured using the MOLA Topography layer in the Java Mission-planning and Analysis for Remote Sensing (JMars) GIS package. Depth measurements were not obtainable, since the scale of these features are below the detection limit of HRSC DTMs. Although there were no HiRISE images of flank vents at the time of this study, there were a couple of the graben. I used the Thermal Emission Imaging System (THEMIS) Daytime infrared global mosaic as a base map. I mapped the vents and arcuate graben in JMars. I used ESRI ArcGIS 10.2 to display the CTX mosaic, identify vents and perform average nearest neighbor analysis. Stereonet 9 was used to project coordinate data onto rose diagrams.

4. Observations

I observed a total of 209 volcanotectonic features on the flanks of Olympus Mons. Here I consider the northeast and southwest flow aprons as part of the Olympus Mons edifice. I identified 125 possible flank vents and 84 arcuate graben. Due to uncertainty in the mode of formation of some features (e.g. features that might resemble flank vents but were formed via other volcanic processes), I ranked them based on my confidence (i.e. high, medium, low, very low) in identifying them as flank vents. My level of confidence increased if there was no observable relationship to other volcanic features. Confidence decreased if features occurred in close proximity to other volcanotectonic features which offered an alternative mode of formation. Features ranked as low and very low are not included in the results discussed in this paper. As a result, I identified

60 flank vents with high to medium confidence. The difference between high and medium confidence was a matter of image quality, DTM availability or definitive morphological characteristics. It is important to note that the inclusion of low and very low confidence vents do not significantly change many of the results or implications of this study because the spatial distribution and relative age of those features are similar to the high- to medium-confidence flank vents. Additional DTMs and higher resolution images (e.g. HiRISE) may help confirm more vents in future work. A breakdown of the types of vents observed are provided in Table 1.

4.1 Flank Vents

Flank vents were identified primarily using their morphology. I considered positive topographic features with radiating flows emanating from a central crater or depression to be flank vents. *Bleacher et al.* [2007] noted that some features previously identified as flank vents on Olympus Mons represent lava fans, positive topographic features formed by lava tube breakouts where changes in slope occurred. I agree that lava fans are a common landform on Olympus Mons. However, I am confident that the features I have identified do not represent lava fans and likely represent places where magma has erupted onto the surface due to subsurface transport via dike or sill propagation. It remains a challenging task to differentiate some features based solely on morphology given the number of overlapping volcanic landforms and the effects of dust on finer scale morphology. Noting morphological and morphometric differences between the 60 vents, I classified the vents into four categories: low shields, fissure vents, cones and lava lakes/other (Fig. 3).

4.1.1 Low shields

Of the 60 vents observed, 42 are classified as low shields. Low shields are positive topographic features with a convex up profile and slopes averaging less than 2 degrees [Greeley, 1977; Greeley, 1982; Hauber et al., 2009]. Low shields are a common landform in the Tharsis province and come in a variety of sizes [Wilson and Head, 1994; Bleacher et al., 2009; Hauber et al., 2009]. The low shields on Olympus Mons might be considered very low shields, since they have heights generally under 100 meters [Hauber et al., 2009]. Based on morphology and morphometry, I further divided the observed shields into 3 subcategories: traditional low shields, non-traditional low shields and transitional shields (Table 2). These categories were created for the purposes of this study.

Traditional low shields agree with the previous definition [Greeley 1977; Greeley, 1982] and display radially emanating, tongue-shaped flows (Fig. 4a). These edifices are built by the repeated effusion of low viscosity lavas. Traditional low shields account for 25 of the 42 low shields observed. The ratio of the width of the summit crater to shield diameter (W_{cr}/W_{co}) ratio has been used in studies of cinder cones, stratovolcanoes and shields to distinguish between volcanic constructs [Wood, 1979; Wood, 1980; Hauber et al., 2009]. I invoke the morphometric ratio to highlight the different morphometries observed between the shields (Table 2). Traditional low shields are slightly larger than their non-traditional counterparts but display a lower W_{cr}/W_{co} ratio of ~ 0.06. This is similar to the terrestrial average of ~0.08, but higher than the Martian average of ~ 0.031 [Wood, 1979; Hauber et al., 2009]. Due to embayment relationships, the diameters measured represent the apparent diameter. Thus, the ratios should be considered absolute

maxima. Traditional shields display no correlation with elevation, however, generally they occur closer to the geographic center of the volcano (~210 – 280 km).

Unlike traditional shields, non-traditional low shields are built by several distinct, overlapping tabular flow lobes giving them a flower petal-like morphology (Fig. 4b) and a higher W_{cr}/W_{co} ratio of ~0.128. The observed ratio is much higher than the terrestrial and Martian averages [Wood, 1979; Hauber et al., 2009]. Although some portion of these shields might be buried beneath embaying flows or obscured by dust, the ratios are much higher than those measured for traditional shields suggesting a possible difference in rheology or development. Indeed, the summit craters are larger than that traditional shields, which may suggest a particular eruption style. Generally, non-traditional low shields occur farther away from the volcanic center (~240 – 320 km). Many non-traditional low shields do occur along the escarpment, which might suggest slope effects play a role.

Transitional low shields are defined as a combination between traditional and non-traditional low shields. These edifices display both morphologies, albeit usually a superposition relationship is observed with traditional shield morphology occurring after, or atop, the flower petal morphology (Fig. 4c). Most of these shields appear to have started with distinct flat flow lobes, and later transitioned to the narrower, tongue-shaped flows of traditional shields. The small number of transitional shields makes statistical analysis less robust. Nevertheless, transitional low shields display an intermediate size between traditional and non-traditional low shields. The W_{cr}/W_{co} ratio is similar to that of low shields. This reflects the tendency for the traditional shield morphology to overprint the earlier morphology of the non-traditional shield.

I interpret non-traditional low shields to represent places where lava erupted only a few times, assuming each lobe reflects one eruptive event. Several of the non-traditional low shields observed occur in pairs or triplets suggesting a similar source or process for their development. At first, the larger crater and higher W_{cr}/W_{co} ratios might suggests these edifices represent a different type of vent that deserves its own category. This argument is somewhat defeated by transitional shields. Transitional low shields are probably formed by changes in the eruption style, frequency and/or longevity. Some traditional low shields may start as non-traditional low shields. That phase may have been buried by later flows. Thus, the different types of low shields are most likely to represent a developmental sequence. On average the low shields on Olympus Mons have volumes of ~0.15 km^3. This represents an underestimate since the true height and diameter of the feature is truncated by embaying flows.

4.1.2 Cones

I observed seven features I have interpreted as cones (Fig. 3c). A few features, which may represent degraded cones, were observed but not included in this study due to the ambiguity of their origin. Cones were identified based on morphology and morphometry (Table 3). They occur at various flank elevations and distances. All cones display embayment relationships with lava flows. Some are almost completely buried. W_{cr}/W_{co} ratios for the cones (~0.15 – 0.4) agree well with Martian (~0.28) and terrestrial (~0.20 – 0.40) values for cinder, or scoria, cones [Wood, 1980; Hauber et al., 2009; Broz and Hauber, 2012]. Our values are overestimates, due to an underestimate of the cone diameter due to lava flow embayment. On this basis, I have interpreted most, if not all, of our cones as cinder cones. HRSC DTM coverage was available for only one cone, but

its height (~10 m) is within the vertical accuracy of the DTM [Jaumann et al., 2007]. Considering height ratios for a degraded cone ($0.13W_{co}$), this particular cone with an apparent diameter of 0.25 km should have a height of ~30 m [Wood, 1979; Wood, 1980]. All of the cones appear degraded and some exhibit asymmetries possibly due to deformation by lava flows. Most are found near other volcanic landforms, such as low shields, fissure vents or lava channels. One cone located on the escarpment is subject to steeper slopes which may have affected its growth and morphological expression.

4.1.3 Fissure Vents

The small number of fissure vents (n = 7) makes statistical analysis unreliable (Fig. 3d). Fissures are observed at a variety of elevations and distances from the volcanic center. Most display a raised rim near the vent. Lava flows are observed emanating from the vents, with preferential flow downhill. One fissure vent was covered by an HRSC DTM on the lower flanks of Olympus Mons. Flows from this vent have constructed a low edifice ($\leq$ 20 m) that tapers off quickly from the vent. The lack of observed fissure vents on the flanks of the shield may reflect burial of these subtle features by later lavas or evolution into low shields.

4.1.4 Lava Lake / Other

This category is reserved for features that did not fit into the previous 3 categories (n = 4). The features in this category are sub-circular depressions that have not built a distinct edifice although flows emanate from them, suggesting lava flowed out at some point (Fig. 3e). Most are filled with dust and aeolian bed forms. No correlation exist between this vent type and flank elevation or distance. As noted earlier, the small sample makes statistical analysis unreliable. Generally, these features are a few hundred meters

across. As with fissure vents, the topographic subtlety of the features offers a probable reason for their rarity.

4.1.5 Flank Vent Spatial Distribution

I measured the elevation of each vent above the surrounding plains and the distance of each vent from the center of the volcanic caldera complex. This is slightly east of the geographic center of the volcano caused by Olympus Mons's asymmetry relative to its calderas. The center of the nested caldera complex was chosen as the center here because direct pathways to the magma chamber below are assumed [Wood, 1984; Thomas et al., 1999; Zuber and Mouginis-Mark, 1992]. Because ~2 km of lava from Tharsis and the Tharsis Montes have embayed Olympus Mons to the east all vent elevation values are referenced to the elevation of the plains west of Olympus Mons which sit at an elevation of – 2.5 km. A few vents clustered together (located $\leq$ 5 km apart). I assigned these vents the same elevation and distance to the center of the volcano. I found a bimodal distribution in flank vent location as a function of elevation (Fig. 5a). Vents occur preferentially at elevations between 8 – 14 km and below 4 km. Flank vents are observed along portions of the escarpment that have been modified to a smaller degree than observed in the northeast and southwest. Thus, vents occurring at elevations lower than ~8 km, occur exclusively on either the flow aprons that drape the escarpment to the northeast and southwest or portions of the scarp that have been mantled by lava flows. No vents are observed above 20 km in elevation. Above 20 km elevation, the terrain has been "smoothed" due to volcanic activity from the summit calderas and possibly the incorporation of dust and volatiles. The location of flank vents as a function of distance from the center of the volcano obeys a more Gaussian distribution (Fig. 5b).

Vents cluster about 200 – 280 km from the center. It is important to note the basal escarpment averages 263 km from the center of the volcano (varying from ~225 km in the east to ~320 km in the northwest). Vents occurring farther out than this distance mostly occur on the flow aprons and portions of the escarpment mantled with lava flows. Figure 6(a) displays the distribution of vents relative to the actual geographic center of the volcano. I also calculated the density of flank vents as a function of distance from the geographic center. Here, I use the actual center of the volcano in order to capture more of the area of the shield. In order to calculate the density of vents (Table 4, Fig. 6b), I approximated Olympus Mons as a circle with a radius of 263 km divided into 6 zones of equal area (~43460 km^2). I found that 78% of flank vents occur within 263 km of the geographic center of the volcano. A third of flank vents occur between 235 – 288 km, on the lowest flank of the volcano, mantled escarpment or flow aprons.

4.1.5.1 Nearest Neighbor Analysis

Nearest neighbor analysis provides a description of the degree of randomness of a population [Clark and Evans, 1954; Bleacher et al., 2009]. It has been used in a variety of studies to characterize the evolution of small volcanic fields by determining the degree of clustering [Bishop, 2008; Bleacher et al., 2009]. If there is no clustering and the volcanic field displays a Random Poisson distribution, this suggests that each vent formed unaffected by the formation of earlier or subsequent vents. A non-random distribution suggests that the vents share a common mode of formation. Terrestrial studies have shown that the spacing of vents can be used a proxy for source depth [Wood, 1980; Bleacher et al., 2009; Hauber et al., 2009]. I found that the flank vents on Olympus Mons display moderate to strong clustering. Given that the vents occur on the flanks of a

shield volcano, this is not surprising and suggests that the vents share a common formation mechanism and/or source region. Initially, I was uncertain whether vents identified on the flow aprons were sourced from Olympus Mons [Bleacher et al., 2009]. The degree of clustering lends credence that even these vents off the main shield are related to volcanism occurring on the edifice and may share a similar source or sources.

4.2 Arcuate Graben

Graben are defined as linear depressions bounded by normal faults, in which the floor has moved down relative to the surrounding terrain. They form as a result of extensional stress. I observed 84 arcuate graben on the flanks of Olympus Mons (Fig. 7). These are small scale features, ranging from 2 – 87 km in length and averaging 120 m in width (Fig. 8a). The graben are observed to be concentric about the center of the edifice. A couple of larger graben are observed on the northeastern flow lobe. These larger graben are similar in scale to some of the graben observed on the Tharsis Montes. I included them in this study since they are concentric and possess a similar spatial relationship as the smaller graben. Due to the small size of the graben, they were not resolvable using HRSC DTMs, suggesting the graben are shallower than 10 m. HiRISE images confirm that these features are topographically subtle, especially at smaller scales, and most have been heavily modified by dust. Over 60% of the graben observed have experienced little or no modification by subsequent volcanism (Fig. 8b). Six have been superposed by sizable impact craters (~0.3 km). Two graben on the southwestern flow apron display ambiguous relationships to pit chains.

4.2.1 Spatial Distribution

Arcuate graben also display a somewhat Gaussian distribution with respect to elevation with most occurring at 2 – 14 km (Fig. 9a). Arcuate graben display a bimodal distribution with respect to distance from the center of the caldera (Fig. 9b). One population of graben occurs at distances of 190 – 240 km while the other occurs at 270 – 310 km. This distribution suggests that graben occur similar distances away from the escarpment upslope and downslope. A number of arcuate graben occur on the northeastern and southwestern flow aprons which skews the results. The paucity of graben from 240 – 270 km is probably due to the escarpment. Either its creation destroyed any previous graben or the current stress field prevents graben formation. A density calculation similar to one performed for flank vents was performed for graben (Table 5). I found that 50% of graben occur within 263 km of the center of the summit caldera. This agrees with the bimodal distribution. Approximately 63% of graben occur more than 235 km out. Figure 10 shows the distribution relative to the geographic center of the volcano. The plot reflects the tendency of graben to occur on the flow aprons and mantled portions of the escarpment. This suggest that the process forming these features is occurring primarily on the lower flanks. A similar trend was observed on Ascraeus Mons by *Byrne et al.* [2012]. Fresher portions of the scarp lack graben.

5.Discussion

Previous studies of Olympus Mons have focused on flank terraces and other volcanic features [Carr et al., 1977; Bleacher et al., 2007; Byrne et al., 2009; Byrne et al., 2012]. In this study, I have focused on the identification and characterization of previously unmapped features, namely flank vents and arcuate graben. Our observations

suggest ongoing volcanotectonic activity for Olympus Mons in the Late Amazonian (≤700 Ma) [Neukum et al., 2004; Werner, 2009; Tanaka et al., 2014]. I interpret a history similar to that observed on other large Martian shields, such as Ascraeus Mons [Bleacher et al., 2009; Byrne et al., 2009; Byrne et al., 2012]. In addition, I find that many of the features observed in this study have occurred post-escarpment formation and represent recent processes in Martian geologic history [Neukum et al., 2004; Bleacher et al., 2007; Werner, 2009; Tanaka et al., 2014]. This has broad implications for vent formation and evolution, surface deformation, subsurface magma propagation and the development of Martian shields.

5.1 Flank Vents

There are more flank vents on Olympus Mons than has been previously recognized. The prevalence of low shields and paucity of other vent types offer two possible explanations: the most recent lavas erupted on Olympus Mons have a low volatile content and/or low viscosity and the preferential destruction of subtle topographic constructs (e.g. fissure vents and lava lakes) by burial beneath lava flows. The first explanation is supported by the northeast and southwest flow aprons and the ubiquitous lava tubes and channels observed on the flanks [Carr, 1973; Carr et al., 1977; Bleacher et al., 2007]. The surface flows of Olympus Mons have been dated as Late Amazonian, specifically 100 – 700 Ma [Neukum et al., 2004; Werner, 2009; Tanaka et al., 2014]. Smaller areas on the shield, notably in the southwest, have been assigned even younger dates of ≤20 Ma, with some flows as young as 5 Ma [Neukum et al., 2004]. Other localized areas on Olympus Mons have been dated as Early Hesperian, ~ 3.8 Ga, suggesting that older parts of the edifice are preserved [Neukum et al., 2004; Werner,

2009]. The flank vents themselves are embayed by lava flows fed primarily by lava channels and tubes [Bleacher et al., 2007]. The prevalence of these features and the lack of edifice construction support the eruption of a low volatile lava on the flanks. The lavas of Olympus Mons have managed to construct a 22 km edifice, evidence of very prolonged volcanic activity. It is plausible that many, if not most, flank vents on the edifice have been buried. The vents I observe today represent a snapshot of the last episode of vent construction.

The observation of cones on Olympus Mons suggests that some of the lavas erupted onto the surface did possess volatiles. I have interpreted the cones I observed as cinder cones. Explosive basaltic volcanism is theorized to be more likely on Mars [Wilson and Head, 1994]. That does not exclude the possibility of other types of cones (e.g. maars, tephra rings and cones). It has been hypothesized that ice may exist beneath a layer of dust and assorted volcanics atop the large Martian shield volcanoes [Tanaka, 1985; Helgason, 1999; Neukum et al., 2004; Bleacher et al., 2007]. The lack of any observable and identifiable phreatomagmatic constructs suggests a lack of recent lava and water interactions. This does not necessarily refute the existence of ice, but may instead point to less volcanism. If the cones observed are cinder cones and I assume the ages on the shield are correct, then they have survived for much longer periods of time than their terrestrial counterparts. Terrestrial cinder cones have a lifespan from birth to death via erosion of a few million years [Hooper and Sheridan, 1998]. The persistence of the cones on Olympus Mons for tens or hundreds of millions of years highlights a fundamental difference in cinder cone evolution on Mars. Cinder cones have been identified in a variety of locations across Mars, but attempts to constrain their ages are ongoing [Broz

and Hauber, 2012]. As for Olympus Mons, it is possible that the persistence of cones for tens or hundreds of millions of years may be due in part to their heavy modification. If the cone is nearly buried by lava flows and mantled by a protective dust layer, then its topographic expression is lessened and the edifice is armored against erosion. Additionally, the processes that cause degradation on Mars are very different from those on Earth. Mars lacks a thick atmosphere, rain and bioturbation. This would result in much lower rates of degradation relative to Earth.

5.2 Spatial Relationship between Flank Vents and Graben

The spatial relationship of flank vents to other features on Olympus Mons allows us to establish a time line for their development. While most vents occur on the main flank of the shield, a fair number of vents occur on or below the escarpment. Vents along the escarpment occur along sections that have been modified by lava flows. This suggests that the renewed volcanic activity responsible for creating the escarpment mantling flows also formed the flank vents. The aureole deposits, material thought to be derived from massive landslides originating from Olympus Mons, have been dated as Middle Amazonian [Tanaka, 1985; Mouginis-Mark and Christensen, 2005; Tanaka et al., 2014]. The vents observed at or below the escarpment formed subsequent to the formation of the escarpment and emplacement of the aureoles and prior to or concurrent with the formation of the scarp mantling flows.

Although I cannot establish whether or not the flank vents occurring above the escarpment pre- or post-date the escarpment, I can constrain vent formation to recent Martian geologic history. The present surface of Olympus Mons has been dated as Late Amazonian, which suggest the flank vents share a similar age [Neukum et al., 2004;

Werner, 2009; Tanaka et al., 2014]. Although mantled in ~1 m of dust, most of the vents observed display a paucity of impact craters and fresh morphologies [Christensen, 1986]. Additionally, none of the vents observed have been buried by subsequent lava flows suggesting they occurred at a time of waning volcanic activity. I do not think the vents are necessarily the youngest expressions of volcanism on the surface of Olympus Mons. Many vents divert flows around them suggesting they were constructed before or concurrent with the emplacement of the effusive flows (Fig. 3b and 4a) [Bleacher et al., 2007].

The superposed arcuate graben on the lower flanks indicates a recent concentric extensional stress field on the edifice [McGovern and Solomon, 1993; Byrne et al., 2012; Weller et al., 2014]. A concentric extensional stress field on the lower flanks is predicted in models that account for large scale volcanotectonic features (e.g. flank terraces, magma chamber, etc.) observed or inferred and allow for gravity spreading [Tanaka, 1985; Thomas et al., 1990; McGovern and Solomon, 1993; Byrne et al., 2009; Byrne et al., 2012]. All observed graben crosscut lower flank flows. Most have experienced little or no modification by later lava flows. Infill due to dust is a larger issue. I cannot rule out the erasure of previous arcuate graben by earlier volcanic activity. In two observed cases restricted to the flow aprons, the graben cut flank vent constructs. In these cases, the graben are younger than the flank vents. However, it is difficult to determine whether or not all the graben are younger than the flank vents. Since the majority of arcuate graben occur more than 235 km from the center of Olympus Mons and the youngest flows occur far from summit, this attests to their young age. The bimodal distribution and density of arcuate graben as a function of distance supports this. I still observe

arcuate graben on the escarpment which indicates that graben have formed post-escarpment formation and modification. The occurrence of graben on portions of the escarpment that have been modified by lavas and the lack of graben on more pristine portions of the escarpment supports the idea that collapse of the shield and creation of the scarp erased any preexisting graben. Consequently, any extensional stress applied to steep slopes of the pristine scarp likely results in localized mass wasting and collapse. Perhaps the presence of mantling lava flows allows the stress to manifest on the surface as graben. Taken together, the evidence suggests arcuate graben are some of the youngest features on Olympus Mons.

5.3 Magma Plumbing System

The age of the Olympus Mons caldera complex has been dated to 100 – 200 Ma [Neukum et al., 2004; Werner, 2009; Tanaka et al., 2014]. This is interpreted to represent the time of the last subsidence of the magma chamber which would correspond with the formation of the caldera floor. Assuming a pressurized chamber and taking into account structural features observed on Olympus Mons (e.g. terraces), the modelled depth of the chamber at the time of subsidence places it within the edifice [Thomas et al., 1990; Zuber and Mouginis-Mark, 1992]. It is unclear how this change in the magma chamber and collapse of the caldera affected volcanism on the flanks. Given that most of the flank is older than this event, only the most recent volcanism on the flanks (e.g. those flows $\leq$ 200 Ma) could have been affected. The clustering of vents suggests either a common driver in their formation and/or shallow source depths of a primary or secondary magma source [Wood, 1980; Bleacher et al., 2009; Pozzobon et al., 2015]. Given the sheer size of Olympus Mons, both of these hypotheses are plausible. The occurrence of flank vents

suggests that radial dikes have propagated hundreds of kilometers [Mouginis-Mark and Christensen, 2005; Byrne et al., 2012]. Models predict that radial dike propagation would be favored assuming a concentric σ-3 stress field [McGovern and Solomon, 1993]. Alternatively, the existence of multiple magma reservoirs within the edifice cannot be ruled out. The clustering of the vents suggests many of the source chambers are likely within the edifice except perhaps for those vents that occur at the lowest elevations. Additionally, dike propagation, in conjunction with a decollement at depth, could also provide a mechanism for flank failure [Elsworth and Day, 1999, Helgason, 1999]. As a result, the process responsible for producing flank vents and sourcing flows on the shield may have helped initiate collapse on the lower flanks of Olympus Mons leading to the formation of the escarpment and associated aureole deposits.

5.4 Late Amazonian Tectonism

Previous studies on Olympus Mons and other large Martian volcanoes have focused on the observed flank terraces [Carr, 1973, Thomas et al., 1990; McGovern and Solomon, 1993; Byrne et al., 2009; Byrne et al., 2012]. These features are interpreted as the surface expression of thrust faulting due to gradual collapse of the edifice [Thomas et al., 1990; McGovern and Solomon, 1993; Byrne et al., 2009; Byrne et al., 2012]. Recently, the focus has shifted to smaller scale features such as pit chains, wrinkle ridges and arcuate graben [Byrne et al., 2009; Byrne et al., 2012; Weller et al., 2014; Pozzobon et al., 2015]. Arcuate graben on the flanks of Olympus Mons suggest an extensional stress regime. This agrees with model predictions assuming gravity spreading [Tanaka, 1985; Thomas et al., 1990; McGovern and Solomon, 1993; Byrne et al., 2009] or flexure of the volcano in response to its own load on the lithosphere [Byrne et al., 2009; Byrne et

al., 2012]. Superposition relationships suggest that the extensional stress regime occurred concurrent with but primarily after the emplacement of flows and vents. This is supported by the lack of significant lava overprinting on the graben and presence of graben on a few vent constructs. The age of the graben are constrained by the surfaces they crosscut. Some graben may be very young, especially those observed on the southwest flow apron, where some flows are dated at ≤20 Ma [Neukum et al., 2004]. I conclude that the observed extensional stress has occurred in the Late Amazonian [Neukum et al., 2004; Werner, 2009; Tanaka et al., 2014]. *Byrne et al.* [2012] proposed that the arcuate graben around Ascraeus Mons might have been formed earlier in the volcanoes evolution, buried by subsequent volcanism and then reactivated. The graben observed around Ascraeus Mons occur not only on the shield but also in the surrounding volcanic plains. No arcuate graben are observed in the plains around Olympus Mons. This does not preclude the possibility of the graben observed on Olympus Mons representing reactivation of earlier tectonism. It is possible Late Amazonian volcanism changed the stress field and reactivated buried faults. Other studies have identified current instability along the scarp in the form of flank collapse due to extension, specifically on the eastern scarp [Weller et al., 2014]. This is supported by concentric compressional features in the plains surrounding Olympus Mons [Weller et al., 2014]. This evidence may suggest an extensional stress field is currently acting on the flanks of Olympus Mons today.

5.5 Development of Martian Shields

The development of Olympus Mons appears similar to that proposed by *Byrne et al.* [2012] for Ascraeus Mons and possibly the other Tharsis Montes. Olympus Mons

underwent an initial shield building stage that began in the Late Noachian or Early Hesperian (~ ≥3.8 Ga) [Werner, 2009; Tanaka et al., 2014]. Like Ascraeus Mons, Olympus Mons was primarily built by effusive lava flows via tubes and channels [Carr, 1973; Carr et al., 1977; Wilson and Head, 2002; Bleacher et al., 2007; Byrne et al., 2012]. This is evidenced by the lack of flank vents observed on each and the dominance of observed lava channels and tubes [Carr, 1973; Carr et al., 1977; Bleacher et al., 2007; Byrne et al., 2012]. Once the edifice reached some height, possibly higher than its current elevation, it underwent gravitational collapse. This caused compression near the summit and produced thrust faults and the observed terraces on the upper flanks [Byrne et al., 2009]. The growth of the shield produced extensional stresses on the lower flanks, and combined with dike propagation and substrate heterogeneity, led to several episodes of flank collapse. This formed the circumferential escarpment and aureole deposits. Afterwards, there was widespread resurfacing via primarily effusive volcanic eruptions [Bleacher et al., 2007]. This created the large flow aprons to the northeast and southwest, similar to the large aprons observed on the Tharsis Montes. Observed flank vents and arcuate graben on Olympus Mons confirms that these features are also a characteristic of large Martian shields. Flank vents played a modest role in the resurfacing. Explosive eruptions on Martian shields played an even smaller role, suggesting volatile poor magmas in recent Martian history. On Olympus Mons, concentric graben developed concurrent with Late Amazonian resurfacing courtesy of an extensional stress field. These graben continued to develop as the volcanic activity waned. Once volcanic and tectonic activity ceased, aeolian deposition of dust dominated the surface of Olympus Mons, punctuated by the occasional meteor impact.

6. Conclusion

Present day Olympus Mons is a product of ~3.8 Ga of volcanic activity. Late Amazonian volcanic resurfacing produced a number of volcanic features, including 60 flank vents. Flank vents have played a limited role in the development of Martian shields. Flank vent morphology suggests that primarily effusive eruptions of low volatile lavas dominated Late Amazonian resurfacing. The identification of cones, however, suggests that limited explosive basaltic eruptions did occur. Flank vent spacing supports radial dike propagation and shallow magma reservoirs within the edifice. The occurrence of vents along the escarpment and on the lava flow aprons indicates that copious volcanic activity has occurred since the formation of the scarp and deposition of the aureoles. This represents renewed growth of the shield. The identification of 84 arcuate graben supports the presence of a concentric stress field on the lower flanks, which promotes faulting and possibly flank collapse. Graben observed cutting the escarpment and lower, and perhaps younger, lava flows suggests recent extension. Previous dating of the calderas and flows on the shield suggests that volcanic activity has occurred very recently and tectonic activity continues on Olympus Mons. The observation of flank vents, arcuate graben and their relationship to other features have allowed us to reconstruct a generalized history for Olympus Mons. Our interpretation agrees well with the development of other large shields on Mars with minor differences unique to Olympus Mons, suggesting similar geologic processes operating across the planet.

References

Bishop, M.A. (2008), Higher-order neighbor analysis of the Tartarus Colles cone groups, Mars: The application of geographical indices to the understanding of cone pattern evolution, *Icarus*, *197*, 73 – 83, doi: 10.1016/j.icarus.2008.04.003.

Bleacher, J.E., R. Greeley, D.A. Williams, S.C. Werner, E. Hauber, G. Neukum (2007), Olympus Mons, Mars: Inferred changes in late Amazonian aged effusive activity from lava flow mapping of Mars Express High Resolution Stereo data, *J. Geophys. Res., 112*, E04003, doi: 10.1029/2006JE002826.

Bleacher, J.E., L.S. Glaze, R. Greeley, E. Hauber, S.M. Baloga, S.E.H. Sakimoto, D.A. Williams, T.D. Glotch (2009), Spatial and alignment analyses for a field of small volcanic vents south of Pavonis Mons and implications for the Tharsis province, Mars, *J. Volcanol. Geotherm. Res., 185*, 96 – 102, doi: 10.1016/j.volgeores.2009.04.008.

Bleacher, J.E., J.A. Richardson, P.W. Richardson, L.S. Glaze, S.M. Baloga, R. Greeley, E. Hauber, R.J. Lillis (2010), Updates to the Catalog of Tharsis Province Small Volcanic Vents, Mars, *Lunar Planet. Sci., XLI*, Abstract 1615.

Blasius, K.R., and J.A. Cutts (1981), Topography of Martian Central Volcanoes, *Icarus, 45*, 87 – 112.

Brož, P., and E. Hauber (2012), A unique volcanic field in Tharsis, Mars: Pyroclastic cones as evidence for explosive eruptions, *Icarus, 218,* 88 – 99, doi: 10.1016/j.icarus.2011.11.030.

Byrne, P.K., B. van Wyk de Vries, J.B. Murray, V.R. Troll (2009), The geometry of volcano flank terraces on Mars, *Earth and Planet. Sci. Lett., 281*, 1 – 13, doi: 10.1016/j.espl.2009.01.043.

Byrne, P.K., B. van Wyk de Vries, J.B. Murray, V.R. Troll (2012), A volcanotectonic survey of Ascraeus Mons, Mars, *J. Geophys. Res., 117,* E01004, doi: 10.1029/2011JE003825.

Carr, M.H. (1973), Volcanism on Mars, *J. Geophys. Res., 78*, 4049 – 4062.

Carr, M.H. (1974), Tectonism and Volcanism of the Tharsis Region of Mars, *J. Geophys. Res., 79, no. 26*, 3942 – 3949.

Carr, M.H., R. Greeley, K.R. Blasius, J.E. Guest, J.B. Murray (1977), Some Martian Volcanic Features as Viewed From the Viking Orbiters, *J. Geophys. Res., 82*, 3985 – 4015.

Christensen, P.R. (1986), Regional Dust Deposits on Mars: Physical Properties, Age, and History, *J. Geophys. Res., 91, no. B3,* 3533 – 3545.

Christensen, P.R., B.M. Jakosky, H.H. Kieffer, M.C. Malin, H.Y. McSween, K. Nealson, G.L. Mehall, S.H. Silverman, S. Ferry, M. Caplinger, M. Ravine (2004), The Thermal Emission Imaging System (THEMIS) for the Mars 2001 Odyssey Mission, *Space Sci. Rev., 110,* 85 – 130.

Clarke, P.J., and F.C. Evans (1954), Distance to the nearest neighbor as a measure of spatial relationships in populations, *Ecology, 35, no. 4,* 445 – 453.

Corrazato, C., and A. Tibaldi (2006), Fracture control on type, morphology and distribution of parasitic volcanic cones: An example from Mt. Etna, Italy, *J. Volcanol. Geotherm. Res., 158,* 177 – 194, doi: 10.1016/j.volgeores.2006.04.018.

Davidson,J., and S. DeSilva (2000), Composite Volcanoes, *Sigurdsson, H. (Ed.), Encyclopedia of Volcanoes, Acad. Press, San Diego,* 663 – 681.

Elsworth, D., and S.J. Day (1999), Flank collapse triggered by intrusion: the Canarian and Cape Verde Archipelagoes, *J. Volcanol. Geotherm. Res., 94,* 323 – 340.

Greeley, R. (1977), Basaltic "Plains" Volcanism, in Greeley, R., and King, J.S., eds., *Volcanism of the eastern Snake River Plain: A Comparative Planetary Geology Guidebook,* NASA CR-154621.

Greeley, R. (1982), The Snake River Plain, Idaho: Representative of a new category of volcanism, *J. Geophys. Res.*, v. *87*, pp. 2705-2712.

Greeley, R., and P.D. Spurdis (1981), Volcanism on Mars, *Rev. of Geophys. Space Phys., 19,* 13 – 41.

Hauber, E., J. Bleacher, K. Gwinner, D. Williams, R. Greeley (2009), The topography and morphology of low shields and associated landforms of plains volcanism in the Tharsis region of Mars, *J. Volcanol. Geotherm. Res., 185,* 69 – 95, doi: 10.1016/j.jvolgeores.2009.04.015.

Helgason, J. (1999), Formation of Olympus Mons and the aureole escarpment problem on Mars, *Geology, 27, no. 3,* 231 – 234.

Hooper, D.M., and M.F. Sheridan (1998), Computer-simulation models of scoria cone degradation, *J. Volcanol. Geotherm. Res., 83,* 241 – 267.

Hulme, G. (1976), The Determination of the Rheological Properties and Effusion Rate of an Olympus Mons Lava, *Icarus, 27,* 207 – 213.

Jaumann, R., G. Neukum, T. Behnke, T.C. Duxbury, K. Eichentopf, J. Flohrer., S. Van Gasselt, B. Giese, K. Gwinner, E. Hauber, H. Hoffmann, A. Hoffmeister, U. Köhler, K.-D. Martz, T.B. McCord, V. Mertens, J. Oberst, R. Pischel, D. Reiss, E. Ress, T. Roatsch, P. Saiger, F. Scholten, G. Schwartz, K. Stephan, M. Wählisch The HRSC Co-Investigator Team (2007), The high-resolution stereo camera (HRSC) experiment on Mars Express: instrument aspects and experiment conduct from interplanetary cruise through the nominal mission, *Planet. Space Sci., 55*, 928 – 952.

King, J.S., and J.R. Riehle (1974), A Proposed Origin of the Olympus Mons Escarpment, *Icarus*, *23*, 300 – 317.

Malin, M.C., J.F. Bell, B.A. Cantor, M.A. Caplinger, W.M. Calvin, R.T. Clancy, K.S. Edgett, L. Edwards, R.M. Haberle, P.B. James, S.W. Lee, M.A. Ravine, P.C. Thomas, M.J. Wolff (2007), Context camera investigation on board the Mars Reconnaissance Orbiter, *J. Geophys. Res., 112*, E05S04, doi: 10.1029/2006JE002808.

McEwan, A.S., E.M. Eliason, J.W. Bergstrom, N.T. Bridges, C.J. Hansen, W.A. Delamere, J.A. Grant, V.C. Gulick, K.E. Herkenhoff, L. Keszthelyi, R.L. Kirk, M.T. Mellon, S.W. Squyres, N. Thomas, C.M. Weitz (2007), Mars Reconnaissance Orbiter's High Resolution Imaging Science Experiment (HiRISE), *J. Geophys. Res., 112*, E05S02, doi:10.1029/2005JE002605.

McGovern, P.J., J.R. Smith, J.K. Morgan, and M.H. Bulmer (2004), Olympus Mons aureole deposits: New evidence for a flank failure origin, *J. Geophys. Res.*, *109*, E08008, doi: 10.1029/2004JE002258.

McGovern, P.J., and S.C. Solomon (1993), State of Stress, Faulting, and Eruption Characteristics of Large Volcanoes on Mars, *J. Geophys. Res., 98, No. E12*, 23,553 – 23,579.

Mouginis-Mark, P.J., and P.R. Christensen (2005), New observations of volcanic features on Mars from the THEMIS instrument, *J. Geophys. Res.*, *110*, E08007, doi: 10.1029/2009JE00241.

Mouginis-Mark, P.J., and S.K. Rowland (2001), The geomorphology of planetary calderas, *Geomorph., 37*, 201 – 223.

Nakamura, K. (1976), Volcanoes as possible indicators of tectonic stress orientation – principle and proposal, *J. Volcanol. Geotherm. Res., 2*, 1 – 16.

Neukum, G., R. Jaumann., H. Hoffmann, H., E. Hauber, J.W. Head, A.T. Basilevsky, B.A. Ivanov, S.C. Werner, S. van Gasselt, J.B. Murray, T. McCord, and The HRSC Co-Investigator Team (2004), Recent and episodic volcanic and glacial activity on Mars revealed by the High Resolution Stereo Camera, *Nature*, 432, 971 – 979.

Plescia, J.B. (2004), Morphometric properties of Martian volcanoes, *J. Geophys. Res., 109,* E03003, doi: 10.1029/2002JE002031.

Pozzobon R., F. Mazzarini, M. Massironi, L. Marinangeli (2015), Self-similar clustering distribution of structural features on Ascraeus Mons (Mars): implications for magma chamber depth, *Geo. Soc., London, Special Publications, 401,* 203 – 218.Rowland, S.K. (1996), Slopes, lava flow volumes, and vent distributions on Volcán Fernandina, Galápagos Islands, *J. Geophys. Res., 101, no. B12,* 27,657 – 27,672.

Tanaka, K.L. (1985), Ice-Lubricated Gravity Spreading of the Olympus Mons Aureole Deposits, *Icarus,* 62, 191 – 206.

Tanaka, K.L., J.A. Skinner, Jr., J.M. Dohm, R.P. Irwin, III, E.J. Kolb, C.M. Fortezzo, T. Platz, G.G. Michael, T.M. Hare (2014), Geologic Map of Mars, *United States Geological Survey*.

Thomas, P.J., S.W. Squyres, M.H. Carr (1990), Flank Tectonics of Martian Volcanoes, *J. of Geophys. Res., 95,* 14,345 – 14,355.

Weller, M.B., P.J. McGovern, T. Fournier, J.K. Morgan (2014), Eastern Olympus Mons Basal Scarp: Structural and Mechanical Evidence for Large Scale Slope Instability, *J. Geophys. Res. Planets, 119,* 1089 – 1109, doi: 10.1002/2013JE004524.

Wilson, L., and J.W. Head IIII (1994), Mars: Review and Analysis of Volcanic Eruption Theory and Relationships to Observed Landforms, *Rev. Geophys., 32, no. 3,* 221 – 263.

Wilson, L., and J.W. Head III (2002), Tharsis-radial graben systems as the surface manifestation of plume-related dike intrusion complexes: Models and implications, *J. Geophys. Res., 107, no. E8,* 5057, doi: 10.1029/2001JE001593.

Wise, D.U., M.P. Golombek, G.E. McGill (1979), Tharsis Province of Mars: Geologic Sequence, Geometry, and a Deformation Mechanism, *Icarus, 38,* 456 – 472.

Wood, C.A. (1979), Monogenetic volcanoes of the terrestrial planets, in *Proc. Lun. Plan. Sci. Conf., 10,* 2815 – 2840, Lunar and Planetary Science Institute, Houston, TX.

Wood, C.A. (1980), Morphometric Evolution of Cinder Cones, *J. Volcanol. Geotherm. Res., 7,* 387 – 413.

Wood, C.A. (1984), Calderas: A Planetary Perspective, *J. Geophys. Res., 89,* 8391 – 8406.

Zuber, M.T., and P.J. Mouginis-Mark (1992), Caldera Subsidence and Magma Chamber Depth of the Olympus Mons Volcano, Mars, *J. Geophys. Res., 97, no. E11*, 18,295 – 18,307.

Zuber, M.T., D.E. Smith, S.C. Solomon, D.O. Muhleman, J.W. Head, J.B. Garvin, J.B. Abshire, J.L. Bufton (1992), The Mars observer laser altimeter investigation, *J. Geophys. Res., 97*, 7781 – 7797.

APPENDIX A

FLANK VENT CLASSIFICATION

Tables

Flank Vent Classification				
	Low Shields	Cones	Fissures	Lava Lakes / Other
Count	42	7	7	4
Average volume (km^3)	~0.15	-	-	-

Table 1: Breakdown of types of flank vents observed on Olympus Mons along with some additional values where possible.

APPENDIX B

MORPHOMETRIC PROPERTIES OF LOW SHIELD FLANK VENTS

Morphometric Properties of Low Shield Flank Vents			
	Traditional	Leaky	Transitional
Count	25	12	5
Average W_{cr} (km)	0.122	0.128	0.15
Average W_{co} (km)	1.67	1.02	1.59
W_{cr}/W_{co}*	0.060	0.128	0.046

Table 2: Properties of different types of low shields observed on Olympus Mons in this study. "*" = ratio is the average of all the W_{cr}/W_{co} measurements taken not the Average in the table. W_{cr} = crater width; W_{co} = cone width.

APPENDIX C

MORPHOMETRIC PROPERTIES OF CONES

Morphometric Properties of Cones							
	1	2	3	4	5	6	7
W_{cr}/W_{co}	0.240	0.150	N/A	0.4	0.250	0.286	0.280

Table 3: W_{cr}/W_{co} ratios for seven cones observed in this study. Cone 2 occurs along the escarpment and has been modified by a channel flow that emerged from its summit. This has altered the crater. Crater on cone 3 is not discernible and may have been degraded.

APPENDIX D

DENSITY OF FLANK VENTS

Flank Vent Density		
Radius (km)	**Percent of Vents**	**Density (vents per 43460 km^2)**
118	5%	3
166	~2%	1
204	~13%	8
235	~32%	19
263	~27%	16
288	~7%	4
Beyond 288	15%	9

Table 4: Density of vents as a function of area. Area between each radius is ~43460 km^2. 263 km is taken as the average distance from the geographic center of the volcano to the escarpment. Percent of Vents refers to the number of vents between stated radius and previous radius divided by the total number of flank vents observed. Values add up to 101% due to rounding.

APPENDIX E

DENSITY OF ARCUATE GRABEN

Arcuate Graben Density		
Radius (km)	**Percent of Graben**	**Density (graben per 43460 km^2)**
118	~3.6%	3
166	~2.4%	2
204	~17%	14
235	~14%	12
263	13%	11
288	~33%	28
Beyond 288	~17%	14

Table 5: Density of graben as a function of area. Area between each radius is ~43460 km^2. 263 km is taken as the average distance from the geographic center of the volcano to the escarpment. Percent of Graben refers to the number of graben between stated radius and previous radius divided by the total number of arcuate graben observed.

Figures

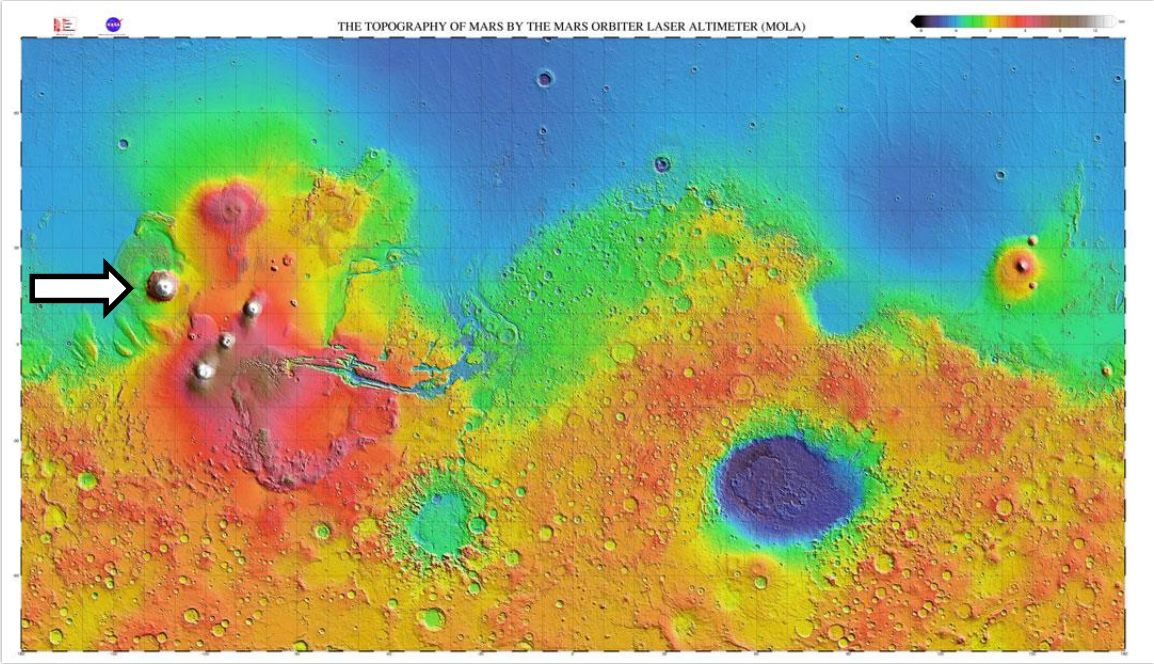

Figure 1: MOLA colorized topographic map of Mars. Warmer colors are higher in elevation. Cooler colors are lower in elevation. White arrow points to Olympus Mons also the highest elevation on Mars. Three white spots to the southeast of Olympus Mons are the Tharsis Montes. Large circular, red sport northeast of Olympus Mons is Alba Mons. Large, dark blue impact basin near bottom of the image is ~2400 km across.

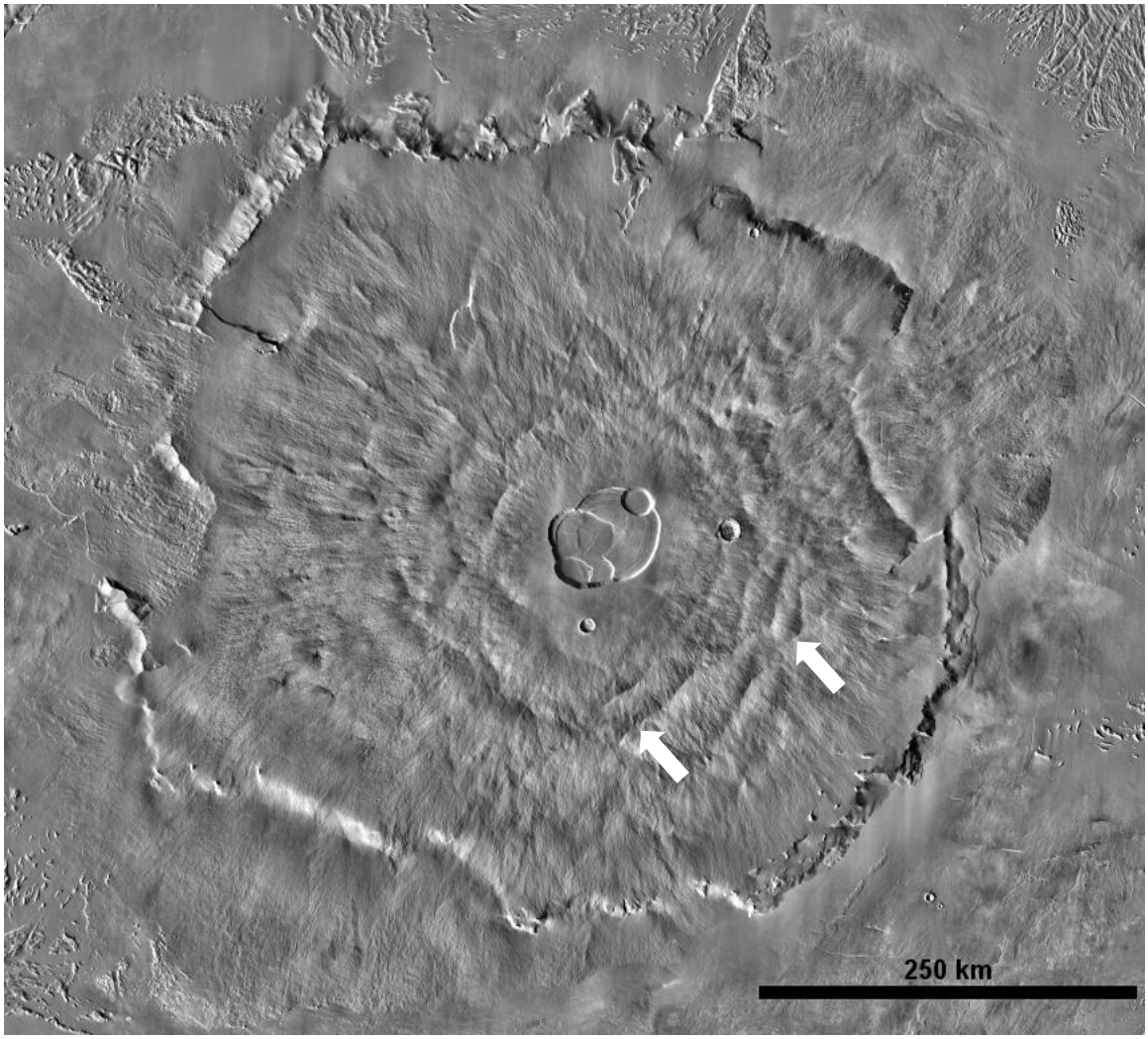

Figure 2: THEMIS Daytime IR mosaic of Olympus Mons. Circular depressions to the south and east of the nested summit calderas are impact craters. Note flow aprons mantling the basal escarpment in the northeast and southwest. Rough material near edges of image are aureole deposits. White arrows point to flank terraces. North is up. Illumination is from the left. Linear discolorations near the scarp are artifacts.

a

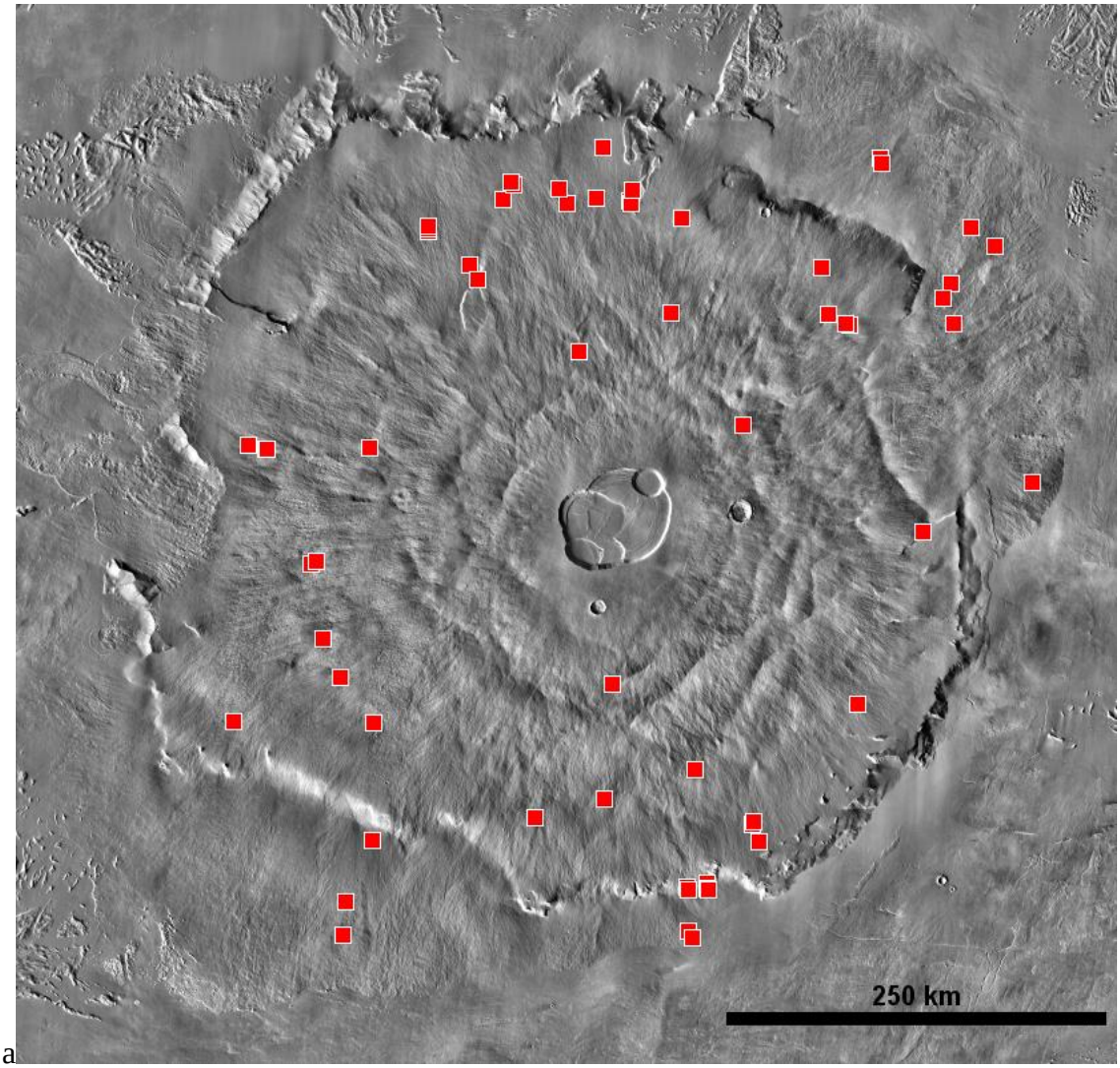

b

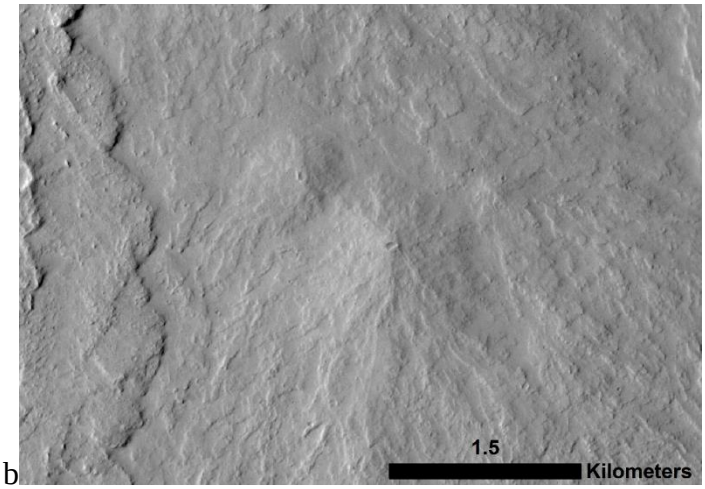

c 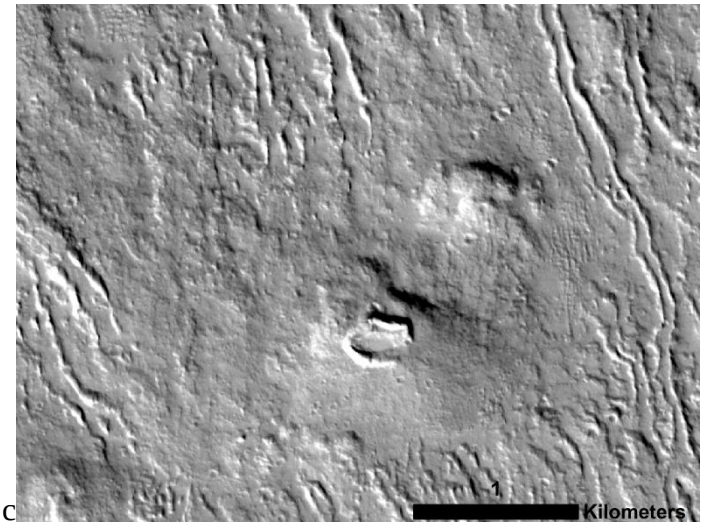

d 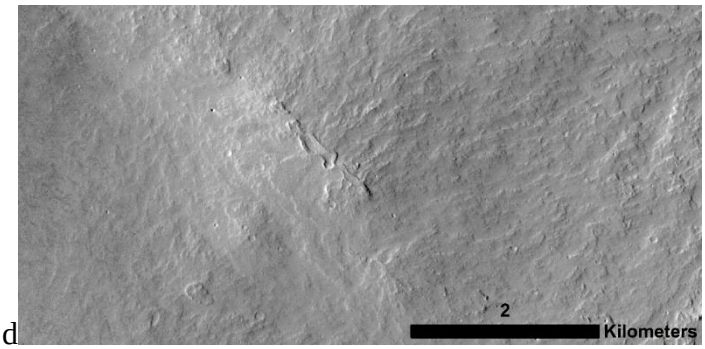

e 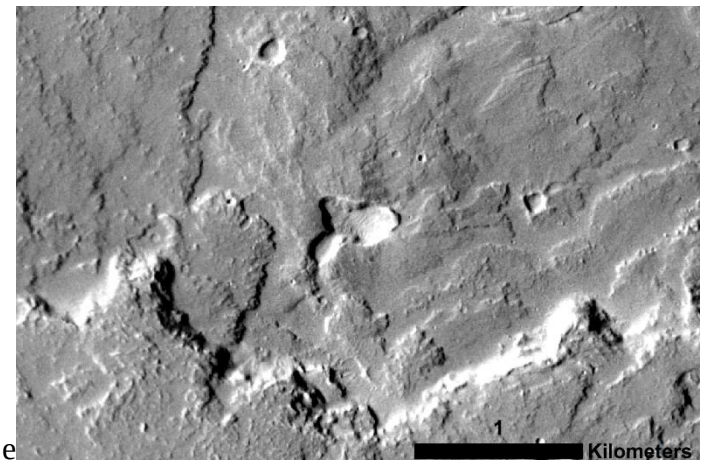

Figure 3: Mapped flank vents on Olympus Mons and examples of each type. North is up in all images. Illumination is from the left in all images. Images b, c and d are all CTX. (a) THEMIS Daytime IR base map. Red squares mark location of vents. Note the occurrence of vents on the flow aprons and mantled portions of the escarpment. There is a paucity of vents observed in the northwest and southeast. (b) Example of two low shields observed along a flow mantled portion of southern escarpment. These represent

traditional low shields. (c) Remnants of a cone. We have interpreted this as a cinder cone, although much of the edifice is embayed with lavas. Lava appears to have spilled into the crater. Mound to the east is interpreted as a landslide or remnants of a cone. (d) A fissure vent on the northeast flow apron. Note the raised edges of the fissure. This fissure appears to have built an edifice. (e) A lava lake on the northeastern flow apron. Flows to the southwest almost buried the feature. Flows appear to emanate from the lava lake and primarily flow to the northeast.

a

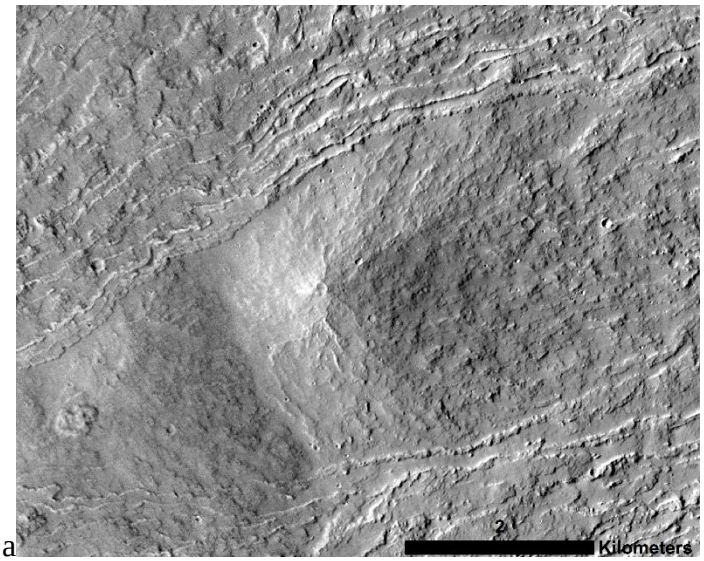

b

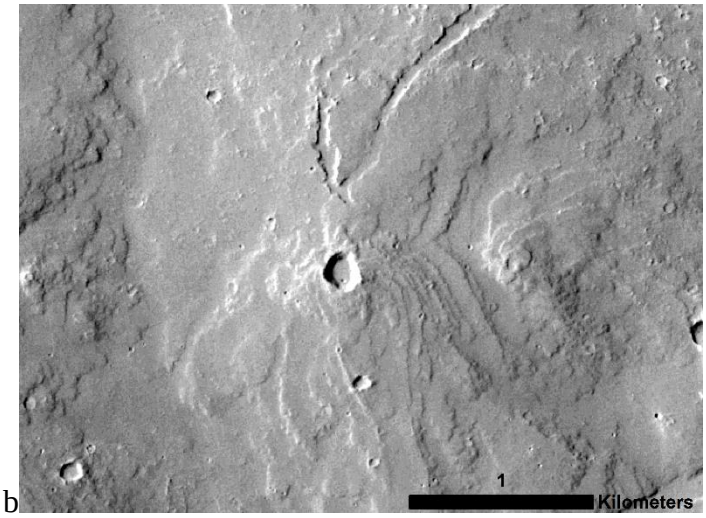

c 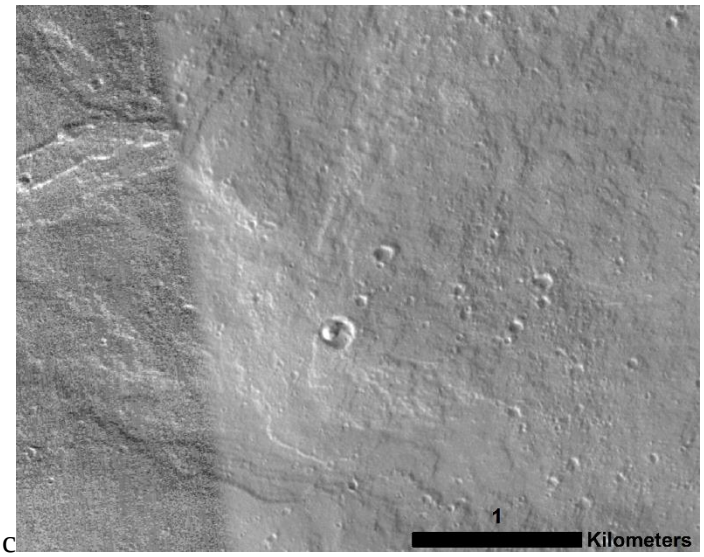

Figure 4: The three types of low shields observed on Olympus Mons. All images are CTX and north is up. Illumination is approximately from the left in all images. (a) Example of a traditional shield on eastern Olympus Mons. Lava flows and channels are diverted around the shield. (b) A leaky low shield. Note the flower petal morphology. Flow units are flat and distinct. A possible secondary vent is located to the east. Fractures to the north may represent fissures or graben. (c) A transition shield. Some flows exhibit flower petal morphology while others do not. An anomalous dome structure is seen in the summit crater. Darker color on the left side of the emission is an artifact.

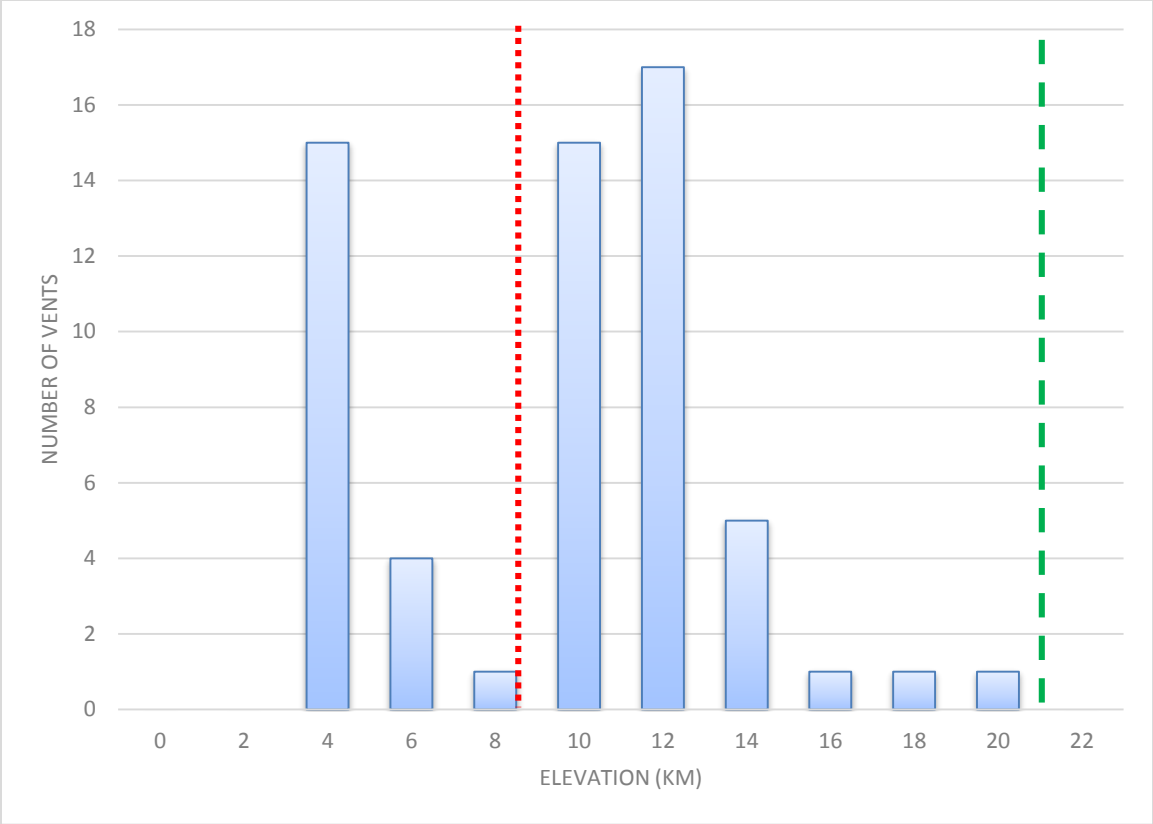
18
16
14
12
10
8
6
4
2
0
NUMBER OF VENTS
0
2
4
6
8
10
12
14
16
18
20
22
ELEVATION (KM)

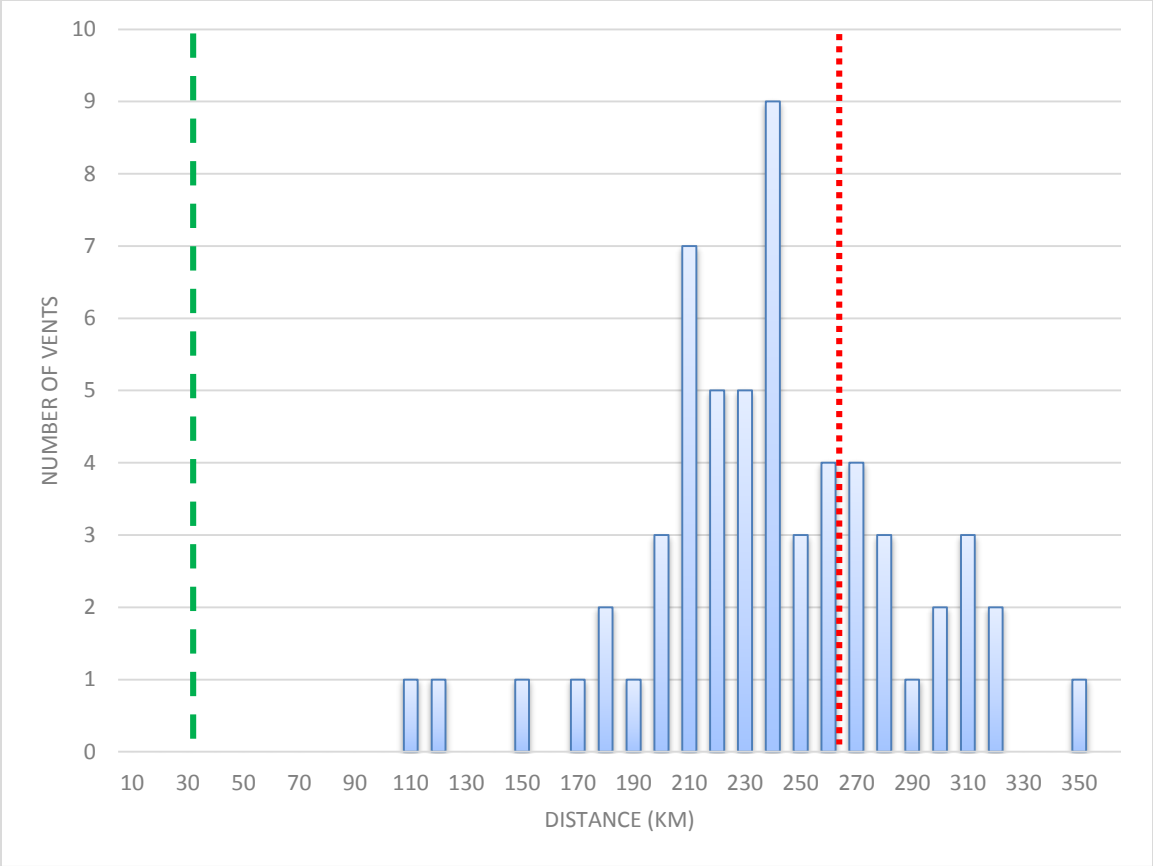

Figure 5: The distribution of flank vents as a function of elevation and distance from the center of the summit calderas. Dotted red line marks the approximate location of the escarpment. Dashed green line denotes approximate edge of the summit calderas. (a) Flank vents display a bimodal distribution, preferentially occurring at 8 – 12 km elevation and ≤ 2km. Vents occurring ≤ 2km occur exclusively on mantled portions of the escarpment, including the flow aprons. (b) Flank vents display a somewhat Gaussian distribution as a function of distance. Vents are found primarily at distances greater than 200 km on the lower flanks of the volcano. This suggest that favorable conditions for eruptions occurred away from the summit, perhaps due to the compressional forces responsible for the flank terraces.

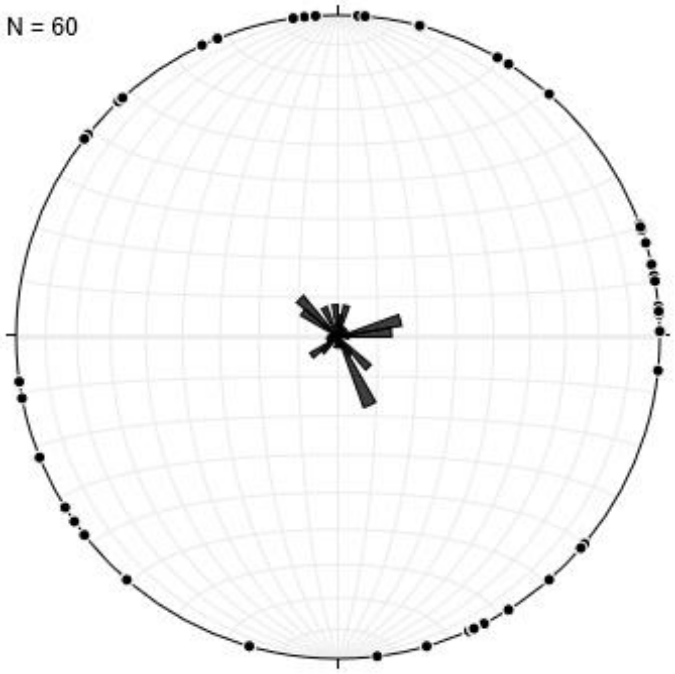
N = 60

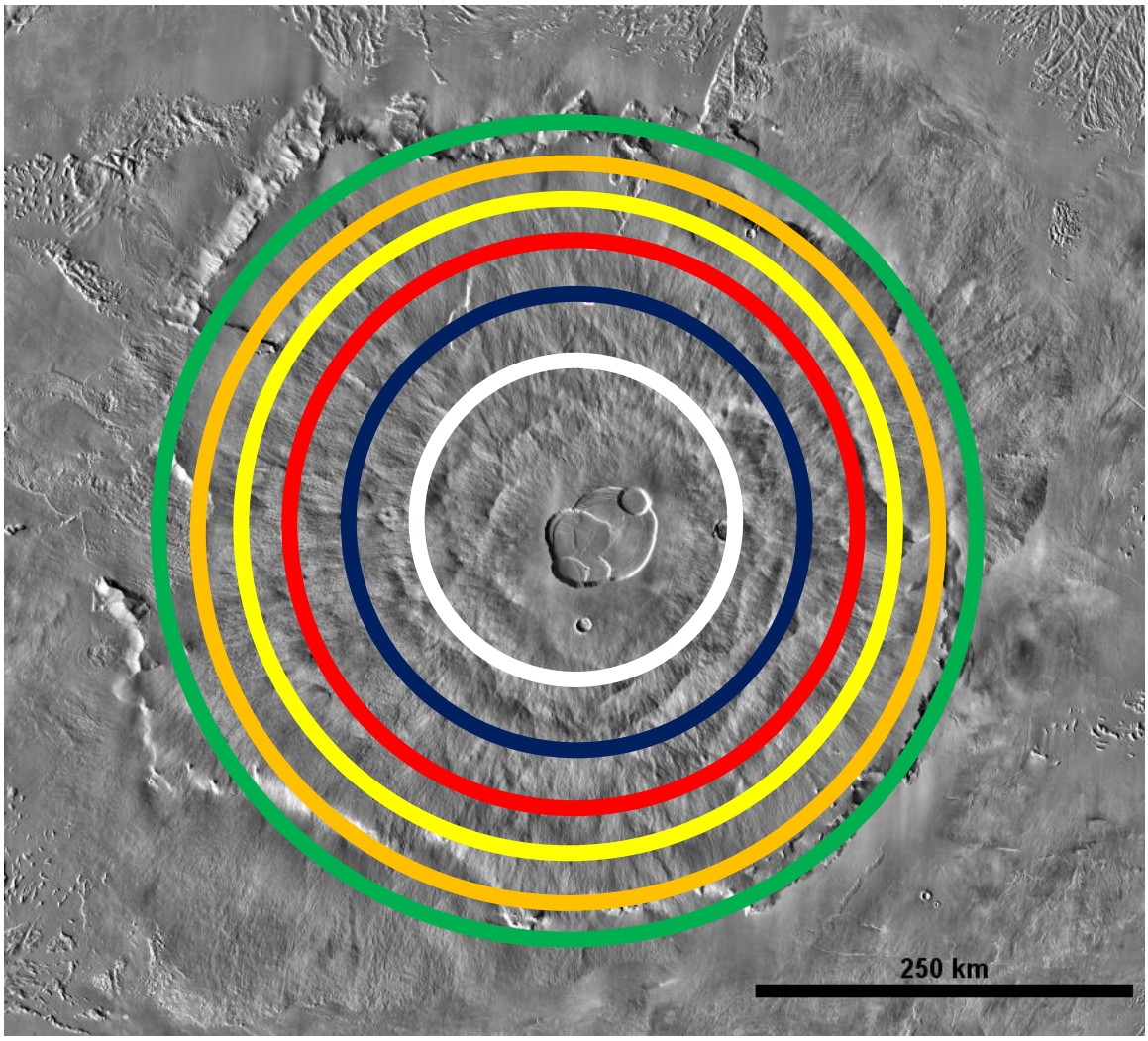

Figure 6: (a) Azimuthal distribution of flank vents relative to the geographic center of the volcano (18.39N, 226.25E). Vents occurring to the northeast and southwest are explained mostly by the flow aprons. The vents occurring to the southeast generally occur on portions of the escarpment that have been mantled by lava flows, similar to the NE and SW. Vents in the northwest occur on the mid to upper flanks. Produced using Stereonet 9. (b) Visual representation of Table 4. Colored circles represent concentric radii used for density calculations. Colors correspond to following radii in km. White = 118; blue = 166; red = 204; yellow = 235; orange = 263; green = 288.

a

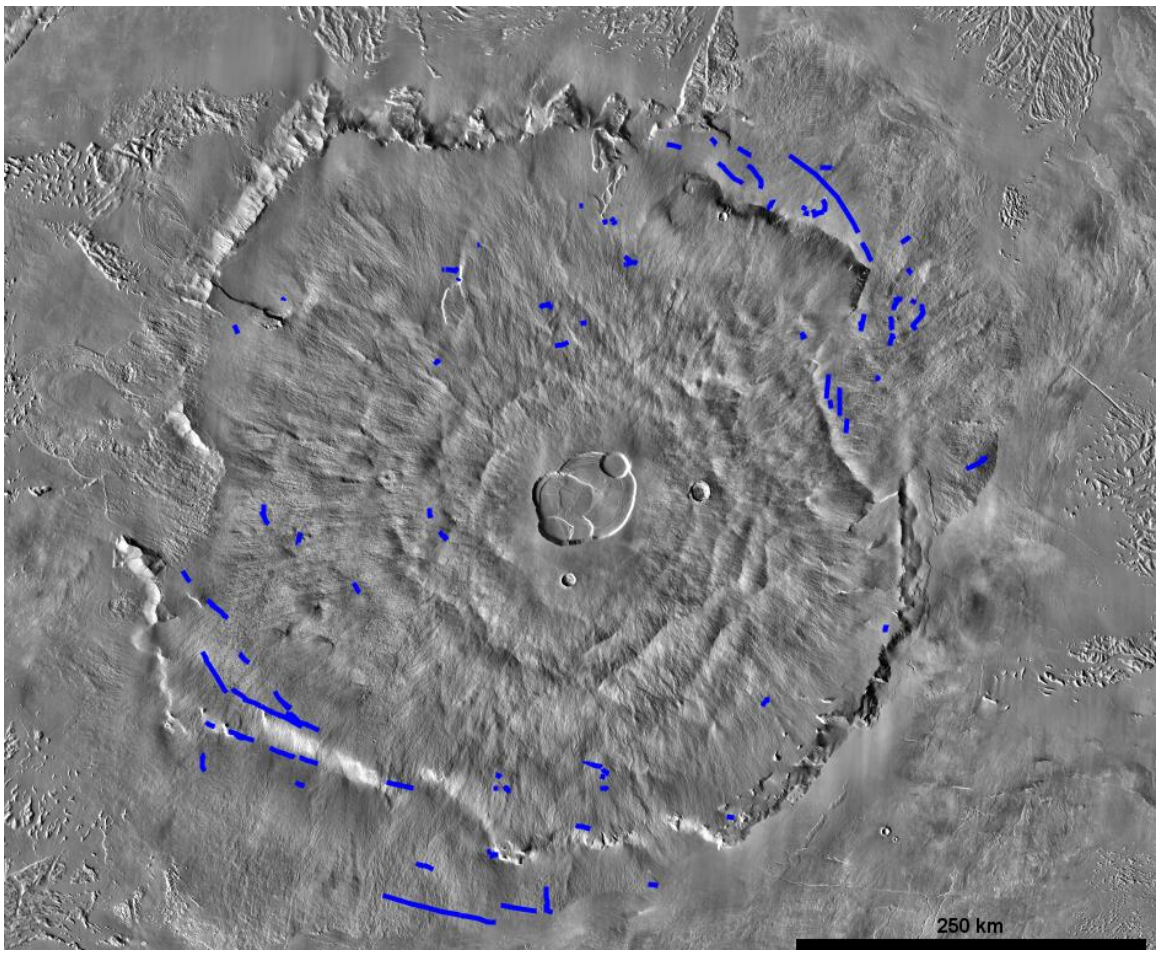

b 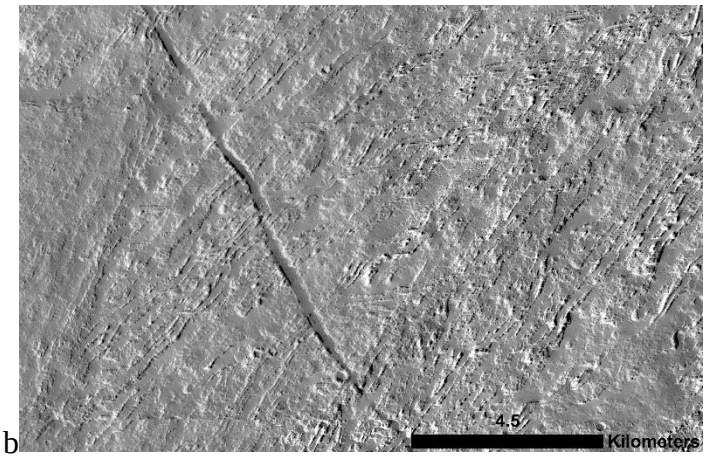

Figure 7: Mapped arcuate graben and example. North is up. Illumination is from the left in both images. (a) Map of 84 arcuate graben observed on Olympus Mons. THEMIS

Daytime IR base map. Blue lines are ~20x wider than average graben. (b) Example of a graben on the southwestern flow apron. Pictured graben is ~150 m wide.

a

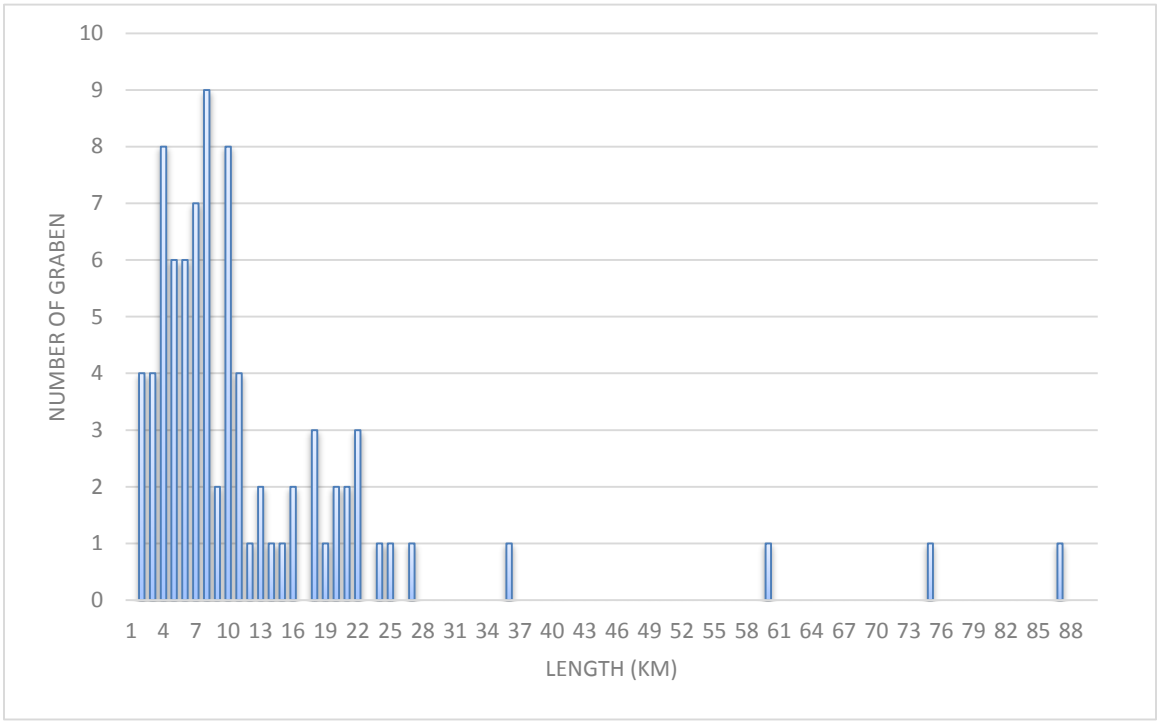
NUMBER OF GRABEN
0
1
2
3
4
5
6
7
8
9
10
1 4 7 10 13 16 19 22 25 28 31 34 37 40 43 46 49 52 55 58 61 64 67 70 73 76 79 82 85 88
LENGTH (KM)

b

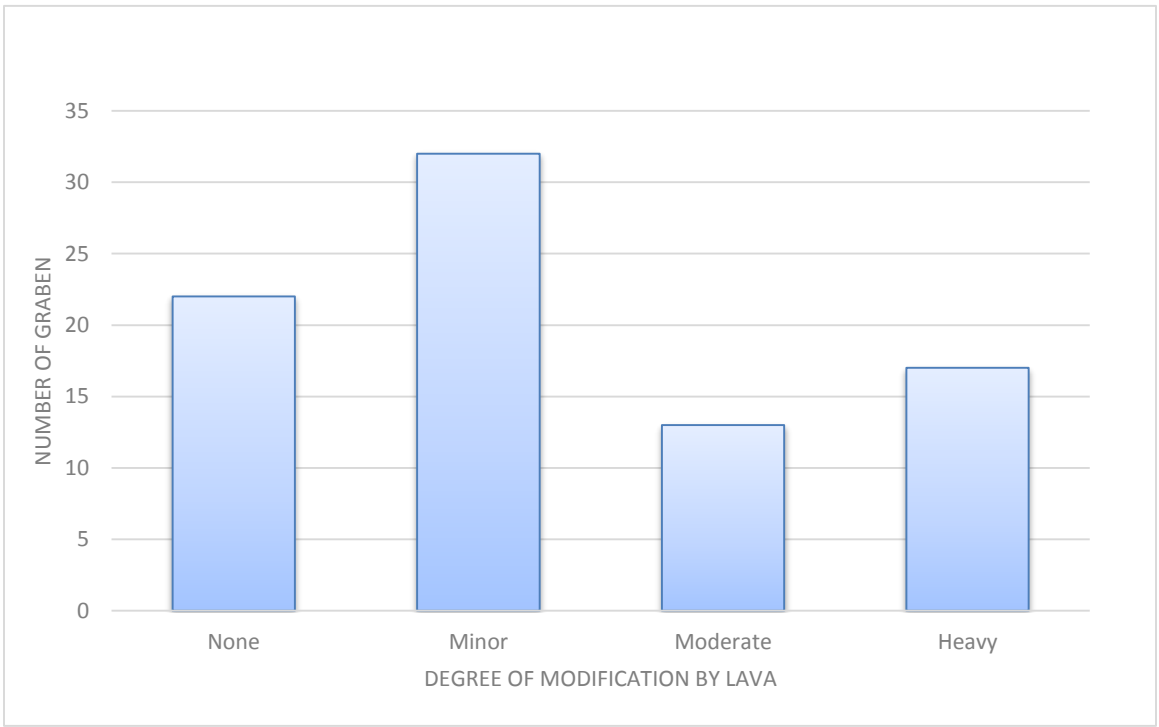
NUMBER OF GRABEN
0
5
10
15
20
25
30
35
None
Minor
Moderate
Heavy
DEGREE OF MODIFICATION BY LAVA

Figure 8: Length distribution and the degree of modification of arcuate graben. (a) Length distribution reveals that generally arcuate graben are small features. (b) Qualitative assessment of the degree of modification by subsequent lava flows.

a

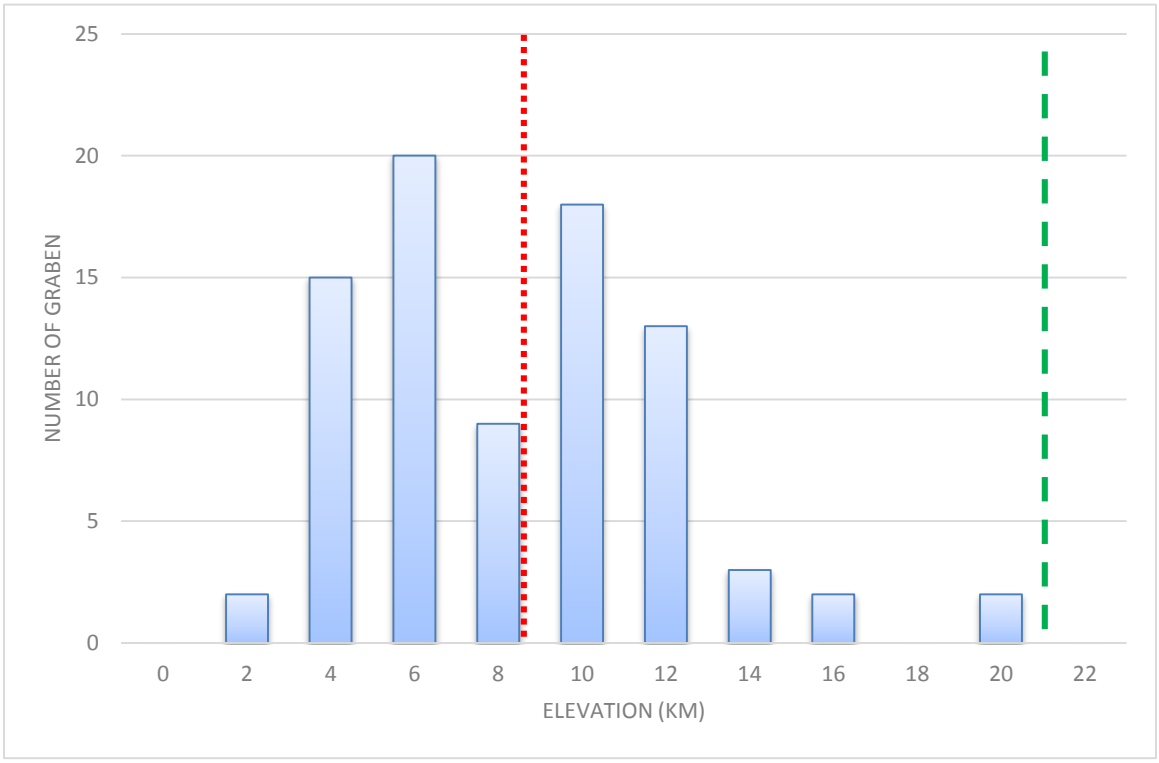
25
20
15
10
5
0
NUMBER OF GRABEN
0
2
4
6
8
10
12
14
16
18
20
22
ELEVATION (KM)

b

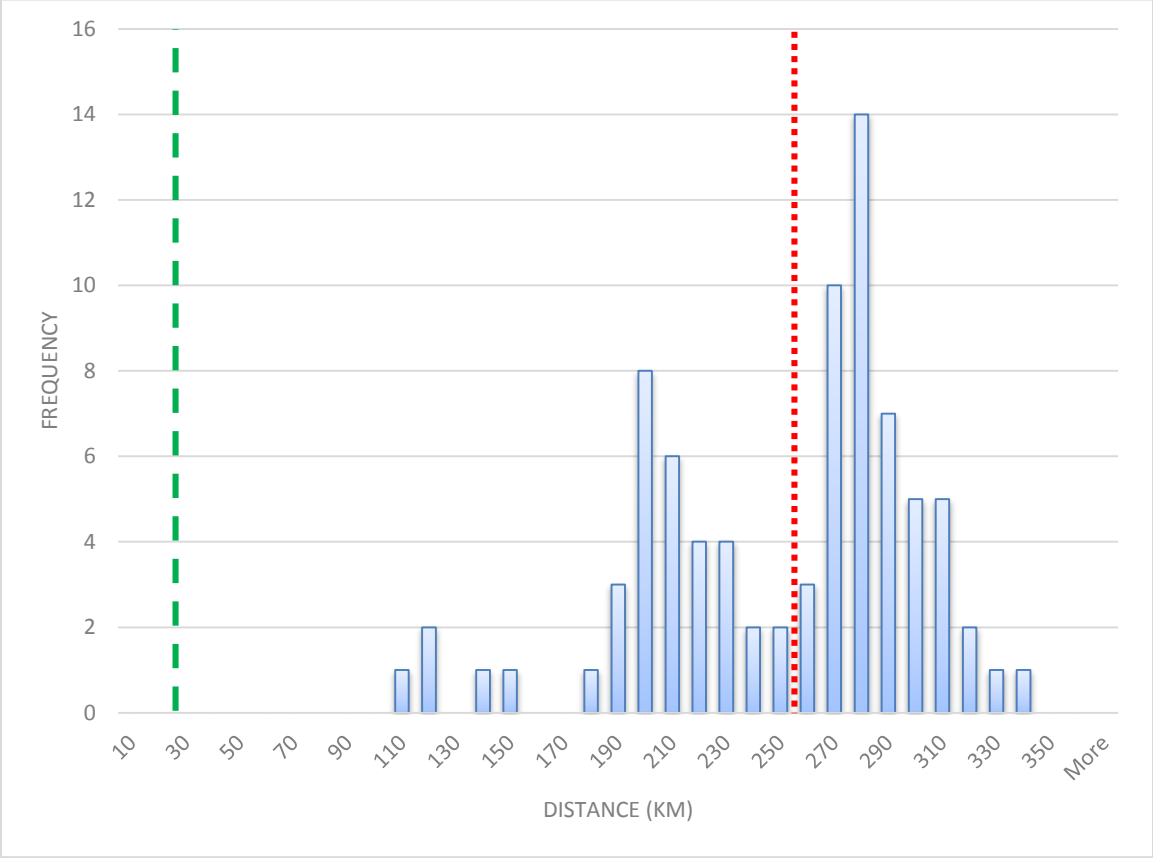

Figure 9: The distribution of graben as a function of elevation and distance from the center of the summit caldera. Red dotted line approximates location of escarpment. Green dashed line approximates edge of summit calderas. (a) Graben display a skewed distribution as a function of elevation, with the likelihood of graben increasing downslope. This suggest that extensional stresses are acting primarily at lower elevations. The dip around 6 km reflects the lack of graben observed at 4 – 6 km, which is mainly due to the escarpment. (b) Graben have a bimodal distribution as a function of distance. The dip corresponds to the escarpment. The distribution suggests that graben are just as likely to form upslope and downslope of the scarp. The graben below the escarpment occur exclusively on the portions of the scarp that have been mantled by lava flows, including the flow aprons.

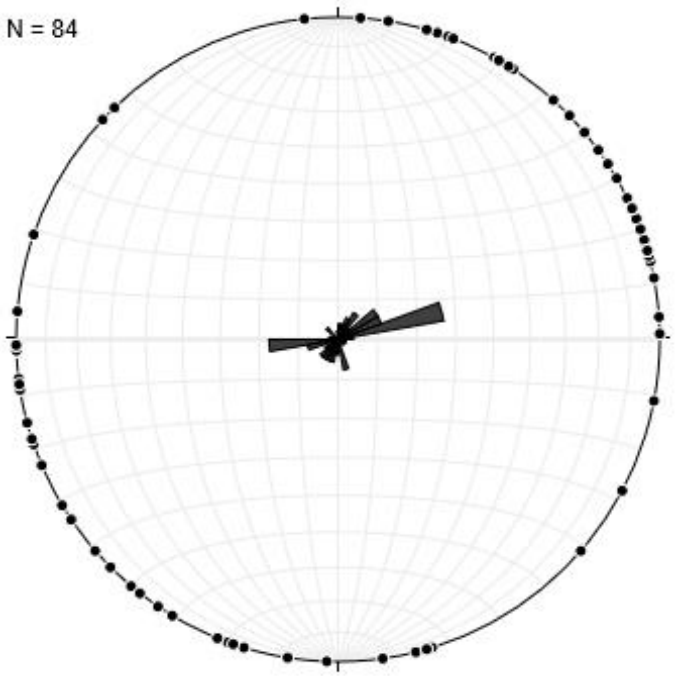

Figure 10: Distribution of arcuate graben relative to the geographic center of Olympus Mons (18.39N, 226.45E). Note the paucity of graben observed to the northwest and southeast. This corresponds to relatively fresh lengths of the escarpment. The distribution is skewed by the preferential occurrence of graben on the northeast and southwest flow aprons. Produced using Stereonet 9.